Journal of Marine Science and Application (2026) 25: 1409-1423
https://doi.org/10.1007/s11804-025-00712-6

RESEARCH ARTICLE

Distributed Adaptive Time-Varying Formation Tracking Regulation Control for USV–UAV Systems

Lei Zhang[1,2], Yixin Cheng[1], Yuxin Zheng[1], Jiayuan Zhuang[1,2] and Renran Zhang[1]

Received: 06 April 2025 / Accepted: 22 July 2025
© Harbin Engineering University and Springer-Verlag GmbH Germany, part of Springer Nature 2026

Abstract
Cooperative control technology has propelled the development of unmanned surface vessel and unmanned aerial vehicle (USV–UAV) systems. To extend their application potential in complex environments, it is essential to improve the flexibility and robustness of time-varying formation tracking (TFT) control for USV–UAV systems. This article proposes a distributed adaptive TFT control scheme with the output regulation theory, such that all vehicles can realize the expected time-varying formation while tracking multiple leaders. First, a distributed observer is constructed to estimate the global states of all leaders. Subsequently, an adaptive TFT controller is presented for each vehicle based on the output regulation framework and the estimated states of the leaders. Given the external disturbances and unknown nonlinearities, system robustness is effectively enhanced by introducing adaptive parameters and compensation inputs. Additionally, extra formation compensation terms are incorporated into the controller to ensure system adaptability to time-varying formation changes. Finally, theoretical analysis and numerical simulations are presented to demonstrate the effectiveness of the proposed scheme.

Keywords Time-varying formation tracking; Adaptive control; Unmanned surface vessels; Unmanned aerial vehicles; Output regulation

1 Introduction

Surface unmanned equipment with excellent autonomy and adaptation, including unmanned surface vessels (USVs) and unmanned aerial vehicles (UAVs) (Barrera et al., 2021; Sendner, 2022), has remarkable value in ocean applications, such as marine exploitation, investigation, and search and rescue over the past decades (Kang et al., 2020; Chang et al., 2021; Johansen et al., 2022). In recent years, the problem of UAV cooperative control has been solved through a number of methods, such as centralized control and distributed control (Ouyang et al., 2023; Yu et al., 2022; Liu et al., 2022). Cooperative control of multiple USVs has captured increasing attention and has been widely applied in marine engineering areas (Huang et al., 2024). To enhance the operational efficiency of maritime tasks, recent research has increasingly focused on USV–UAV systems (Shao et al., 2019; Bi et al., 2024; Tian et al., 2024). Compared to UAVs or USVs system that are composed of homogeneous platforms, such systems exhibit broader surveillance coverage, increased reconnaissance precision, and greater operational flexibility.

Formation control plays a crucial role in ensuring effective task execution for USV–UAV systems and has become an essential area of research (Li et al., 2023a), which needs to force the overall system into a presupposed formation pattern. However, compared with swarm systems composed of either USVs or UAVs, the strong dynamic differences between USVs and UAVs, such as spatial inconsistencies, different damping sources, and actuator types, pose exceptional challenges for the formation control of the system (Gonzalez-Garcia et al., 2021). To drive the USV−UAV systems along the desired trajectories with the desired shape, the dynamics of UAVs were projected onto the horizontal plane, and distributed tracking controllers for USVs and UAVs have been designed independently by Wang and Ahn (2021). Based on platform grouping, the time-varying formation tracking (TFT) control issue was effectively resolved with guiding and programming algorithms (Li et al., 2022a; 2022b; 2022c). To further simplify the control structure and enhance the flexibil-

Article Highlights

- A TFT control scheme for USV–UAV systems is developed based on the output regulation theory.
- A distributed observer is designed to estimate the state information of multiple leaders.
- Adaptive compensations are designed based on radial basis function neural networks and the expected time-varying formation.

✉ Yuxin Zheng
zhengyuxin@hrbeu.edu.cn

[1] National Key Laboratory of Autonomous Marine Vehicle Technology, Harbin Engineering University, Harbin 150001, China

[2] Yangtze Delta Region Advanced Research Institute of Harbin Engineering University, Nantong 226000, China

ity of USV−UAV system collaboration, virtual USVs and UAVs were introduced to program reference routes (Li et al., 2023b). However, the controllers depended on the guidance and planning procedure, which imposes restrictions on the number of vehicles and the formation shape of the system. For this issue, a distributed formation control with a UAV as the leader center was proposed by Liu et al. (2023). The aforementioned research yielded positive outcomes in coordinated control and proposed novel methods for USV–UAV system control.

Fortunately, despite the challenge of matching the internal states of each member in heterogeneous systems, the outputs are often identical (Dong and Hu, 2017). On this basis, output regulation theory was widely applied to deal with the cooperative control problems of full heterogeneous linear systems (Zhang et al., 2019; Hua et al., 2019; Jiang et al., 2022), which unifies the control law design for different members with regulatory equations. To enhance control performance under external disturbances, a distributed proportional–integral control law is proposed for heterogeneous systems by Lv et al. (2018) and Xu et al. (2019). Nevertheless, the aforementioned solutions primarily focus on traditional linear agents, and the USV−UAV systems exhibit strong nonlinear characteristics, which makes cooperative control for heterogeneous systems challenging (Du et al., 2020). In addition, the dynamic model parameters of USVs and UAVs are difficult to fetch in practical scenarios (Qin et al., 2022; Khalid et al., 2023), which further exacerbates the difficulty in designing a controller with the output regulation theory for USV–UAV systems. In light of this situation, universal approximation systems, such as fuzzy systems (Bounemeur et al., 2019; Bounemeur and Chemachema, 2025; Chen et al., 2020), have been widely adopted in the control of nonlinear systems. However, fuzzy control relies on expert knowledge for rule design (Bounemeur and Chemachema, 2021). The strong coupling of the system and disturbances caused by the complicated external environment considerably limits the applicability of fuzzy logic for USV–UAV systems. Therefore, methods to solve the TFT robust control problem for USV–UAV systems under uncertain external disturbances need to be investigated.

Motivated by the aforementioned discussions and analysis, this article focuses on developing a unified scheme of TFT control for USV–UAV systems subject to external disturbance with the output regulation theory. The heterogeneous system can achieve the target time-varying formation along the trajectories of multiple leaders. First, a distributed observer is developed for each vehicle to estimate the states of all leaders. Furthermore, an adaptive TFT regulation control structure is developed. Through dynamic transformation, the regulation control scheme is applied to the USV–UAV system effectively. The main striking superiorities of this paper are described as follows:

1) Different from the existing control methods of USV–UAV systems (Li et al., 2022a; 2022b; Li et al., 2023b), the proposed approach provides a unified control law design method for heterogeneous vehicles, where the tedious coordinated guidance procedure is not required anymore, which simplifies the control structure to some extent. Compared with the existing output regulation methods (Zhang et al., 2019; Jiang et al., 2022), adaptive compensations are introduced to deal with the time-varying formation and mitigate the effects of nonlinearities and unknown external disturbances. In this way, the control schemes can adapt to a wide range of engineering scenarios.

2) The proposed observer enables each node to acquire the global states of the reference center, which are determined by the time-varying positions of the leaders. Moreover, with the combination of the observer and the output regulation controller, this control structure avoids platform-specific grouping for TFT (Li et al., 2022c; Liu et al., 2023). Thus, this control structure balances the roles of USVs and UAVs within the system, facilitating the flexible configuration of time-varying formations.

This paper is organized as follows: Section 2 provides the control problem formulation and some preliminaries. Section 3 discusses the main results of the adaptive TFT regulation controller for the USV−UAV system and presents the proof process in detail. Section 4 showcases the simulation results to illustrate the validity and advantages of the control scheme. Finally, Section 5 concludes this paper.

Variables and formulas

Throughout this paper, let $\mathbb{R}^{n\times m}$ represent a real matrix with $n \times m$ dimension and the operator $\otimes$ represent the Kronecker product. $\mathbf{1}_N$ and $\mathbf{0}_N$ are applied to denote a column vector consisting of the elements 1 and 0 with size N, respectively. $\boldsymbol{I}_n$ represents an identity matrix with dimension n. A diagonal matrix is symbolized as $\mathrm{diag}\{\cdot\}$. Let $\boldsymbol{R} > 0$ denote a positive definite matrix, and $\lambda_{\max}(\boldsymbol{R})$ and $\lambda_{\min}(\boldsymbol{R})$ are used to represent the maximum and minimum eigenvalues of this matrix, respectively. Let the superscript T represent the transpose of a matrix, and $\|\cdot\|$ denote the Euclidean norm. The hyperbolic tangent function of $\boldsymbol{x} = \left[x_1, x_2, \cdots, x_n\right]^{\mathrm{T}} \in \mathbb{R}^n$ is expressed as $\tanh(\boldsymbol{x}) = \left[\tanh(x_1), \tanh(x_2), \cdots, \tanh(x_n)\right]^{\mathrm{T}}$. The function linespace $\left(\alpha_1, \alpha_2, \beta\right)$ is used to generate an equally spaced vector, where α_1 is the upper bound, α_2 is the lower bound, and β is the interval.

2 Preliminaries and problem formulation

2.1 Graph theory

This paper considers a TFT system with M agents marked from 1 to M and N virtual leaders marked from $M + 1$ to $M + N$. A graph $G = \{Q, E, W\}$ is applied to describe the

interactive relationship within the system, where $Q = \{q_1, q_2, \cdots, q_M, \cdots, q_{M+N}\}$ is the node set and $E \subseteq \{(q_i, q_j) | q_i, q_j \in Q, i \neq j\}$ is the edge set. Let $e_{ij} = (q_i, q_j)$ denote the directed edge from q_i to q_j, and q_i is called a neighbor of q_j. The overall neighbors of q_i are defined by the neighbor set $N_i = \{q_j \in Q | e_{ji} \in E\}$. $\boldsymbol{W} = [w_{ij}] \in \mathbb{R}^{(M+N)\times(M+N)}$ denotes the adjacency matrix, and the adjacency element of $\boldsymbol{W}$ satisfies $w_{ij} > 0$ if and only if $e_{ji} \in E$, and $w_{ij} = 0$ otherwise. If $e_{ij} \in E$ implies $e_{ji} \in E$ and $w_{ij} = w_{ji}$, then the graph G is said to be undirected. An undirected graph is connected if there is a path between any two nodes. The Laplacian matrix of G is defined as $\boldsymbol{L} = \boldsymbol{D} - \boldsymbol{W}$, where $\boldsymbol{D}$ is diagonal with $d_i = \sum_{j=1}^{N+M} w_{ij}$, $i \in Q$. Based on the leader–follower structure, the M agents within the system are defined as followers. Let $\Upsilon_F = \{1, 2, \cdots, M\}$ and $\Upsilon_L = \{M+1, M+2, \cdots, M+N\}$ represent the follower and leader subscript sets, respectively.

Assumption 1. The interaction topology among the USVs and UAVs is undirected and connected. In addition, the follower system can receive messages from each leader, which indicates that $\sum_{i=1}^{M} w_{ij} > 0$ is satisfied for the leader $j(j \in \Upsilon_L)$.

Remark 1. Given the difference in mission payload and communication status, only a part of the agents within the USV–UAV system can obtain external information, such as the states of the leaders. However, USVs and UAVs can realize effective information exchange through short-distance communication networks. Therefore, Assumption 1 is reasonable and necessary for USV–UAV systems.

2.2 Mathematical modeling of the USV–UAV system

Consider a USV–UAV system composed of n_s underactuated USVs and $M - n_s$ quadrotor UAVs. For convenience, the models of USVs and UAVs in the system are described under two Cartesian coordinate frames (the earth-fixed frame $O_E X_E Y_E Z_E$ and the body-fixed frame $O_b X_b Y_b Z_b$) as shown in Figure 1.

By referring to Wu et al. (2023), the kinematics of the underactuated USV i in the horizontal plane can be represented as follows:

$$\begin{cases} \dot{x}_{s,i} = u_{s,i}\cos\varphi_{s,i} - v_{s,i}\sin\varphi_{s,i} \\ \dot{y}_{s,i} = u_{s,i}\sin\varphi_{s,i} + v_{s,i}\cos\varphi_{s,i} \\ \dot{\varphi}_{s,i} = r_{s,i} \end{cases} \tag{1}$$

where $i = 1, \cdots, n_s$ is the label of each USV. Let $\boldsymbol{\eta}_{s,i} = [x_{s,i}, y_{s,i}, \varphi_{s,i}]$ denote the state vector with the position $(x_{s,i}, y_{s,i})$ and the yaw angle $\varphi_{s,i}$ of the USV in the navigation frame. $x_{s,i} = [u_{s,i}, v_{s,i}, r_{s,i}]$ represents the velocity vector containing the linear velocities and yaw angular rate in the body-fixed frame. Given the external disturbances, the dynamic model of the USV can be expressed as follows:

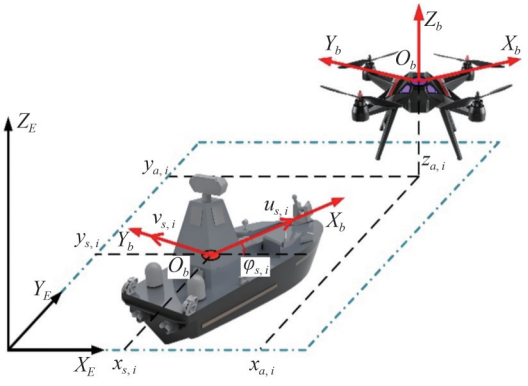


Figure 1 Reference frames of the USV–UAV system

$$\begin{cases} \dot{u}_{s,i} = \left(m_{22,i}v_{s,i}r_{s,i} - d_{11,i}u_i + f_i + d_{x,i}\right)/m_{11,i} \\ \dot{v}_{s,i} = \left(-m_{11,i}u_{s,i}r_{s,i} - d_{22,i}v_{s,i} + d_{y,i}\right)/m_{22,i} \\ \dot{r}_{s,i} = \left(\left(m_{11,i} - m_{22,i}\right)u_{s,i}v_{s,i} - d_{33,i}r_{s,i} + T_i + d_{\varphi,i}\right)/m_{33,i} \end{cases} \tag{2}$$

where $m_{11,i}$, $m_{22,i}$, and $m_{33,i}$ are the inertia and added masses of the USV and $d_{11,i}$, $d_{22,i}$, and $d_{33,i}$ are the hydrodynamic damping parameters. Moreover, f_i/T_i denotes the control force/torque for surge/yaw motion and $[d_{x,i}, d_{y,i}, d_{\varphi,i}]^{\mathrm{T}}$ represents the unknown external disturbances.

The simplified schematic of the quadrotor UAV i $(i = n_s + 1, n_s + 2, \cdots, M)$ with cruciform structure in the formation is presented in Figure 1. The specific position and Euler angles are denoted by $\boldsymbol{\chi}_{a,i} = [x_{a,i}, y_{a,i}, z_{a,i}]^{\mathrm{T}}$ and $\boldsymbol{k}_{a,i} = [\phi_{a,i}, \theta_{a,i}, \varphi_{a,i}]^{\mathrm{T}}$, respectively. Following Song et al. (2018), the nonsimplified dynamic model can be expressed as follows:

$$\begin{cases} \ddot{x}_{a,i} = \left(\sin\phi_{a,i}\sin\varphi_{a,i} + \cos\phi_{a,i}\sin\theta_{a,i}\cos\varphi_{a,i}\right)u_{1,i}/m_{a,i} - \\ \qquad \zeta_{x,i}\dot{x}_{a,i}/m_{a,i} + d_{1,i} \\ \ddot{y}_{a,i} = \left(\cos\phi_{a,i}\sin\theta_{a,i}\sin\varphi_{a,i} - \sin\phi_{a,i}\cos\varphi_{a,i}\right)u_{1,i}/m_{a,i} - \\ \qquad \zeta_{y,i}\dot{y}_{a,i}/m_{a,i} + d_{2,i} \\ \ddot{z}_{a,i} = \left(\cos\theta_{a,i}\cos\phi_{a,i}\right)u_{1,i}/m_{a,i} - g - \zeta_{z,i}\dot{z}_{a,i}/m_{a,i} + d_{3,i} \\ \ddot{\phi}_{a,i} = u_{2,i}/I_{x,i} + \dot{\theta}_{a,i}\dot{\varphi}_{a,i}\left(I_{y,i} - I_{z,i}\right)/I_{x,i} - \zeta_{\phi,i}\dot{\phi}_{a,i} + d_{4,i} \\ \ddot{\theta}_{a,i} = u_{3,i}/I_{y,i} + \dot{\phi}_{a,i}\dot{\varphi}_{a,i}\left(I_{z,i} - I_{x,i}\right)/I_{y,i} - \zeta_{\theta,i}\dot{\theta}_{a,i} + d_{5,i} \\ \ddot{\varphi}_{a,i} = u_{4,i}/I_{z,i} + \dot{\phi}_{a,i}\dot{\theta}_{a,i}\left(I_{x,i} - I_{y,i}\right)/I_{z,i} - \zeta_{\varphi,i}\dot{\varphi}_{a,i} + d_{6,i} \end{cases} \tag{3}$$

where $m_{a,i}$ is the mass of the UAV, g is the gravitational acceleration; $I_{x,i}$, $I_{y,i}$, and $I_{z,i}$ represent the inertia coefficients, and $\zeta_{k,i}, (k = x, y, z, \phi, \theta, \varphi)$ denotes the aerodynamic coefficient. In addition, $u_{k,i}\ (k = 1, 2, 3, 4)$ and $d_{\jmath,i}(\jmath = 1, 2, \cdots, 6)$ represent the control inputs and environmental disturbances, respectively. The following assumption for external disturbances is employed in this paper.

Assumption 2. The unknown external disturbances of the USVs and UAVs are bounded and satisfy $\|d_{k,i}\| \leqslant \bar{d}_{s,k}(k = x, y, \varphi)$ and $\|d_{\jmath,i}\| \leqslant \bar{d}_{a,\jmath}(\jmath = 1, 2, \cdots, 6)$, where $\bar{d}_{s,k}$ and $\bar{d}_{a,\jmath}$ are unknown positive constants.

To simplify the TFT problem of USV–UAV systems, multiple linear virtual leaders are introduced. The dynamic of the leader j is described as follows:

$$\begin{cases} \dot{\boldsymbol{v}}_j(t) = \boldsymbol{S}\boldsymbol{v}_j(t) \\ \boldsymbol{p}_j(t) = \boldsymbol{F}\boldsymbol{v}_j(t) \end{cases} \tag{4}$$

where $\boldsymbol{v}_j(t) \in \mathbb{R}^{n_L}$ and $\boldsymbol{p}_j(t) \in \mathbb{R}^2$ represent the global state and position output, respectively. $\boldsymbol{S}$ and $\boldsymbol{F}$ are the known constant matrices for all virtual leaders, which determine the movement of the leaders.

Remark 2. Marine environmental activities, such as wind and waves, always change with finite energies (Yu et al., 2022; Qin et al., 2022); thus, it is reasonable to set the external disturbances of agents as Assumption 2. The linear leaders are widely used in output regulation issues (Zhang et al., 2019; Hua et al., 2019; Jiang et al., 2022). Alternatively, the leaders are just employed to guide the USVs and UAVs to move along the expected trajectory in this paper. Based on these two points, the leaders are modeled in Equation (4). By adjusting the matrix $\boldsymbol{S}$, the navigation trajectory of the USV–UAV system can be effectively set.

2.3 Control objective

Considering the difference between USV and UAV in internal states or control characteristics, we focus on the position control of each agent. The objective of this paper is to design an adaptive controller for a USV–UAV system to track the expected time-varying formation.

The expected time-varying formation structure can be specified by $\boldsymbol{h}_i(t) \in \mathbb{R}^{n_L}$ that is required to be piecewise continuously differentiable. The target formation position offset $\boldsymbol{\Delta}_i(t) \in \mathbb{R}^2$ is yielded as $\boldsymbol{\Delta}_i(t) = \boldsymbol{F}\boldsymbol{h}_i(t)$. It is worth noting that the formation structure vector has the same dimension as the global state of multiple virtual leaders based on the output regulation theory. The formation is only known by the corresponding agent i.

For any bounded initial state, if $\boldsymbol{p}_i(t) - \boldsymbol{\Delta}_i(t) - \mathcal{P}_L(t) \to 0$ holds for every agent, the system is considered to have achieved the time-varying formation. $\boldsymbol{p}_i(t)$ is the horizontal position of the agent i, $\boldsymbol{\Delta}_i(t)$is the relative formation position offset, and $\mathcal{P}_L(t)$ is the desired trajectory determined by multiple leaders.

Remark 3. $\mathcal{P}_L(t) = \sum_{j=M+1}^{M+N} \rho_j \boldsymbol{p}_j(t), \left(\sum_{j=M+1}^{M+N} \rho_j = 1, \rho_j > 0 \right)$ represents the desired trajectory generated by the reference center of multiple leaders, which can be any point in the convex combination of multiple leaders with different ρ_j. All USVs and UAVs remain at the desired position offsets relative to the reference center when formations are formed. For example, if there exists only one leader, the reference center represents this leader. By changing the desired formation shape and trajectories of the leaders, a more flexible control effect can be achieved, compared to cooperative path following (Li et al., 2023b).

2.4 Related lemmas

Preceding the design of the TFT regulation control protocol, the ensuing lemmas, which will be utilized in the forthcoming sections, are presented.

Lemma 1 (Godsil and Royle, 2013). For the Laplacian matrix of an undirected connected graph, there is a simple eigenvalue $\lambda_1 = 0$ associated with the eigenvector $\mathbf{1}_N$ and $\lambda_k > 0\ (k = 2, 3, \cdots, N)$ without loss of generality.

Lemma 2 (Zhang, 2006; Schur complement). For a given symmetric matrix $\boldsymbol{R} = \begin{bmatrix} \boldsymbol{R}_{11} & \boldsymbol{R}_{12} \\ \boldsymbol{R}_{12}^{\mathrm{T}} & \boldsymbol{R}_{22} \end{bmatrix} \in \mathbb{R}^{n \times n}$, where $\boldsymbol{R}_{11} \in \mathbb{R}^{r \times r}$, the following conditions are equivalent:

1) $\boldsymbol{R} < 0$;
2) $\boldsymbol{R}_{11} < 0, \boldsymbol{R}_{22} - \boldsymbol{R}_{12}^{\mathrm{T}} \boldsymbol{R}_{11}^{-1} \boldsymbol{R}_{12} < 0$;
3) $\boldsymbol{R}_{22} < 0, \boldsymbol{R}_{11} - \boldsymbol{R}_{12} \boldsymbol{R}_{22}^{-1} \boldsymbol{R}_{12}^{\mathrm{T}} < 0$.

Lemma 3 (Wu et al., 2023). For the arbitrary smooth function $f(\boldsymbol{x}):\mathbb{R}^n \to \mathbb{R}^m$, the radial basis function neural networks (RBFNN) with k neurons can be applied to approximate it. The network output is expressed as $f(\boldsymbol{x}) = \boldsymbol{W}^{\mathrm{T}} \mathcal{G}(\boldsymbol{x}) + \boldsymbol{\varepsilon}$. According to the minimum learning parameter (MLP) algorithm , the RBFNN output satisfies :

$$\|f(\boldsymbol{x})\| \leqslant \|\boldsymbol{W}^{\mathrm{T}}\| \|\mathcal{G}(\boldsymbol{x})\| + \|\boldsymbol{\varepsilon}\| \leqslant \Gamma\gamma(\boldsymbol{x}) + R \tag{5}$$

where $\boldsymbol{x} \in \mathbb{R}^n$ represents the input vector, $\boldsymbol{W} \in \mathbb{R}^{k \times m}$ denotes the weight matrix, and $\boldsymbol{\varepsilon} \in \mathbb{R}^m$ is the approximate error. $\mathcal{G}(\boldsymbol{x}) = [g_1(\boldsymbol{x}), g_2(\boldsymbol{x}), \cdots, g_k(\boldsymbol{x})]^{\mathrm{T}}$ represents the basis function output vector of the hidden layer expressed as $g_j(\boldsymbol{x}) = \exp\left(-(\boldsymbol{x} - \mathbf{c}_j)^{\mathrm{T}}(\boldsymbol{x} - \boldsymbol{c}_j) / 2\ell_j^2\right)(j = 1, 2, \cdots, k)$, where $\boldsymbol{c}_j \in \mathbb{R}^n$ is the Gaussian basis function center point vector and ℓ_j refers to the width of the basis function. For brevity, denote $\boldsymbol{c} = [\boldsymbol{c}_1, \boldsymbol{c}_2, \cdots, \boldsymbol{c}_k]$. Based on the MLP algorithm, the maximum norms of the learning parameters are employed, where $\Gamma = \|\boldsymbol{W}^{\mathrm{T}}\|$, $\gamma(\boldsymbol{x}) = \|\mathcal{G}(\boldsymbol{x})\|$, and R is a positive design parameter.

3 Main results

In this section, we present the TFT control scheme for USV–UAV system. The schematic diagram is illustrated in Figure 2. First, the redefined states of USVs and the double-loop control structures for UAVs are introduced to construct the unified formal like-linear models for the USV–UAV system. Then, a distributed observer for each agent is employed to estimate the states of the leaders.

Furthermore, the TFT regulation control protocol and adaptive laws are proposed for the USV–UAV system based on the output regulation theory and MLP-based RBFNN algorithm. Finally, it is proved that the desired time-varying formation can be realized under external disturbances.

3.1 Model transformation

Notably, only two control inputs (f_i, T_i) are provided for the USV; there is no input acting on the sway motion. Thus, the USV model is regarded as underactuated. To deal with this issue and simplify the development of the control protocol, the redefined states are employed for USV $i\,(i = 1, 2, \cdots, n_s)$ by combining the positions and yaw as follows:

$$\begin{cases} p_{x,i} = x_{s,i} + l_i \cos\varphi_{s,i} \\ p_{y,i} = y_{s,i} + l_i \sin\varphi_{s,i} \end{cases} \tag{6}$$

where l_i is a designed parameter, and this change is a translation of the origin in the body-fixed frame. Then, the dynamics of the USV i can be expressed as follows:

$$\begin{cases} \ddot{p}_{x,i} = f_{x,i} + f_i \cos\varphi_{s,i}/m_{11,i} - l_i T_i \sin\varphi_{s,i}/m_{33,i} + \\ \qquad d_{x,i}\cos\varphi_{s,i}/m_{11,i} - d_{y,i}\sin\varphi_{s,i}/m_{22,i} - \\ \qquad l_i d_{\varphi,i}\sin\varphi_{s,i}/m_{33,i} \\ \ddot{p}_{y,i} = f_{y,i} + f_i \sin\varphi_{s,i}/m_{11,i} + l_i T_i \cos\varphi_{s,i}/m_{33,i} + \\ \qquad d_{x,i}\sin\varphi_{s,i}/m_{11,i} + d_{y,i}\cos\varphi_{s,i}/m_{22,i} + \\ \qquad l_i d_{\varphi,i}\cos\varphi_{s,i}/m_{33,i} \end{cases} \tag{7}$$

where

$$\begin{aligned} f_{x,i} = {} & (m_{22,i}v_{s,i}r_{s,i} - d_{11,i}u_{s,i})\cos\varphi_{s,i}/m_{11,i} - u_{s,i}r_{s,i}\sin\varphi_{s,i} - \\ & \left(\left(-m_{11,i}u_{s,i}r_{s,i} - d_{22,i}v_{s,i}\right)/m_{22,i}\right)\sin\varphi_{s,i} - \\ & l_i\left(\left(m_{11,i} - m_{22,i}\right)u_{s,i}v_{s,i} - d_{33,i}r_{s,i}\right)\sin\varphi_{s,i}/m_{33,i} - \\ & v_{s,i}r_{s,i}\cos\varphi_{s,i} - l_i r_{s,i}^2\cos\varphi_{s,i} \\ f_{y,i} = {} & (m_{22,i}v_{s,i}r_{s,i} - d_{11,i}u_i)\sin\varphi_{s,i}/m_{11,i} + u_{s,i}r_{s,i}\cos\varphi_{s,i} + \\ & \left(\left(-m_{11,i}u_{s,i}r_{s,i} - d_{22,i}v_{s,i}\right)/m_{22,i}\right)\cos\varphi_{s,i} + \\ & l_i\left(\left(m_{11,i} - m_{22,i}\right)u_{s,i}v_{s,i} - d_{33,i}r_{s,i}\right)\cos\varphi_{s,i}/m_{33,i} - \\ & v_{s,i}r_{s,i}\sin\varphi_{s,i} - l_i r_{s,i}^2\sin\varphi_{s,i} \end{aligned} \tag{8}$$

To simplify the model, we defined the input transformation matrix as follows:

$$\boldsymbol{\Omega}_i = \begin{bmatrix} \cos\varphi_{s,i}/m_{11,i} & -l_i\sin\varphi_{s,i}/m_{33,i} \\ \sin\varphi_{s,i}/m_{11,i} & l_i\cos\varphi_{s,i}/m_{33,i} \end{bmatrix} \tag{9}$$

which satisfies $\boldsymbol{\Omega}_i^{-1} = \begin{bmatrix} m_{11,i}\cos\varphi_{s,i} & m_{11,i}\sin\varphi_{s,i} \\ -m_{33,i}\sin\varphi_{s,i}/l_i & m_{33,i}\cos\varphi_{s,i}/l_i \end{bmatrix}$, and obtained the following expression:

$$\begin{bmatrix} u_{x,i} \\ u_{y,i} \end{bmatrix} = \boldsymbol{\Omega}_i \begin{bmatrix} f_i \\ T_i \end{bmatrix} \tag{10}$$

Therefore, the USV model can be rewritten as follows:

$$\begin{cases} \ddot{p}_{x,i} = f_{x,i} + u_{x,i} + d_{1,i} \\ \ddot{p}_{y,i} = f_{y,i} + u_{y,i} + d_{2,i} \end{cases} \tag{11}$$

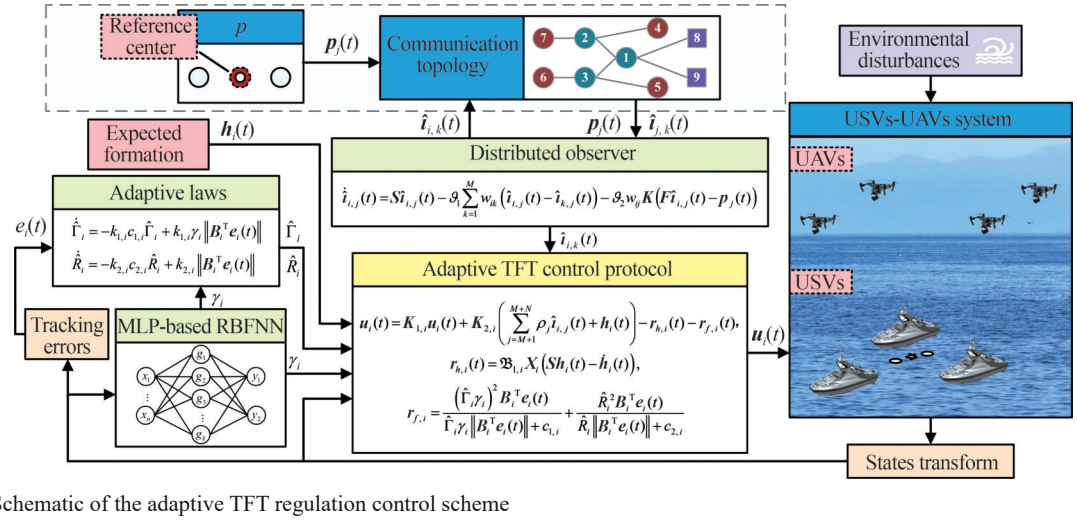


Figure 2 Schematic of the adaptive TFT regulation control scheme

where the redefined disturbances are described as follows:

$$\begin{cases} d_{1,i} = d_{x,i}\cos\varphi_{s,i}/m_{11,i} - d_{y,i}\sin\varphi_{s,i}/m_{22,i} - \\ \qquad l_i d_{\varphi,i}\sin\varphi_{s,i}/m_{33,i} \\ d_{2,i} = d_{x,i}\sin\varphi_{s,i}/m_{11,i} + d_{y,i}\cos\varphi_{s,i}/m_{22,i} + \\ \qquad l_i d_{\varphi,i}\cos\varphi_{s,i}/m_{33,i} \end{cases} \tag{12}$$

Remark 4. Based on the output redefinition, $p_{x,i}$ and $p_{y,i}$ are defined as the formation position of each USV, instead of $x_{s,i}$ and $y_{s,i}$. This approach allows us to focus on the essential formation position control. Nevertheless, an excessively large l_i may lead to unacceptable TFT control errors, whereas a smaller l_i results in control input escalation. Thus, a trade-off is necessary for selecting l_i.

Given the hovering states of the UAVs, which indicate that the attitude angles and angular velocities are small enough, and $u_{1,i} \approx m_i g$, if the TFT problem focuses on the formation position of each member within the USV–UAV system, then the control of the altitude and attitude of the UAV can be disregarded in this paper. Thus, the UAV model expressed in Equation (3) can be simplified as follows:

$$\begin{cases} \ddot{x}_{a,i} = u_{x,i} - \zeta_{x,i}\dot{x}_{a,i}/m_{a,i} + d_{1,i} \\ \ddot{y}_{a,i} = u_{y,i} - \zeta_{y,i}\dot{y}_{a,i}/m_{a,i} + d_{2,i} \end{cases} \tag{13}$$

where $u_{x,i} = \left(\phi_{a,i}\sin\varphi_{a,i} + \theta_{a,i}\cos\varphi_{a,i}\right)g$ and $u_{y,i} = \left(\theta_{a,i}\sin\varphi_{a,i} - \phi_{a,i}\cos\varphi_{a,i}\right)g$ are the virtual inputs for horizontal movement.

Remark 5. The UAV can be controlled with the double-loop structure. The outer loop focuses on the position, whereas the inner loop ensures the desired attitude tracking of the UAV body (Zain, 2011), which places high demands on the inner-loop response performance. In addition, the transition of the UAV model effectively enhances the simplicity of the analysis. However, the simplified conditions for the hovering states constrain the values of the attitude and altitude of the UAV. As a consequence, the controllability of the UAV degrades during the altitude change phase, and the control effectiveness may be compromised when dealing with rapidly changing formation configurations.

The differences in model composition and driving modes between different agents would compromise the design of the TFT control protocol. Based on the aforementioned operations, the relative degree and matching of the USV–UAV system are increased considerably. Then, the formation control model of the agent i in the USV–UAV system can be described as follows:

$$\begin{cases} \dot{\boldsymbol{\mu}}_i(t) = \boldsymbol{A}_i\boldsymbol{\mu}_i(t) + \boldsymbol{B}_i\left(\boldsymbol{\mu}_i(t) + \boldsymbol{d}_i(t) + \boldsymbol{f}_i(t)\right) \\ \boldsymbol{p}_i(t) = \boldsymbol{C}_i\boldsymbol{\mu}_i(t) \end{cases} \tag{14}$$

where $\boldsymbol{\mu}_i(t)$, $\boldsymbol{p}_i(t)$, $\boldsymbol{u}_i(t)$, $\boldsymbol{d}_i(t)$, and $\boldsymbol{f}_i(t)$ are the reference state, output vector, virtual control input, disturbance input, and nonlinear uncertain term, respectively. Given that the TFT problem focuses on the position of each member, the position vectors have the same dimension. The TFT control model of the USV–UAV system can be described concretely. For the USV $i\left(i = 1, 2, \cdots, n_s\right)$,

$$\begin{aligned} \boldsymbol{\mu}_i(t) &= \left[p_{x,i}(t), \dot{p}_{x,i}(t), p_{y,i}(t), \dot{p}_{y,i}(t)\right]^{\mathrm{T}} \\ \boldsymbol{p}_i(t) &= \left[p_{x,i}(t), p_{y,i}(t)\right]^{\mathrm{T}} \\ \boldsymbol{u}_i(t) &= \left[u_{x,i}(t), u_{y,i}(t)\right]^{\mathrm{T}} \\ \boldsymbol{d}_i(t) &= \left[d_{1,i}(t), d_{2,i}(t)\right]^{\mathrm{T}} \\ \boldsymbol{f}_i(t) &= \left[f_{x,i}(t), f_{y,i}(t)\right]^{\mathrm{T}} \\ \boldsymbol{A}_i &= \boldsymbol{I}_2 \otimes \begin{bmatrix} 1 & 0 \\ 0 & 0 \end{bmatrix} \\ \boldsymbol{B}_i &= \boldsymbol{I}_2 \otimes \begin{bmatrix} 0 \\ 1 \end{bmatrix} \\ \boldsymbol{C}_i &= \boldsymbol{I}_2 \otimes \begin{bmatrix} 1 & 0 \end{bmatrix} \end{aligned} \tag{15}$$

For the UAV $i\left(i = n_s + 1, n_s + 2, \cdots, M\right)$,

$$\begin{aligned} \boldsymbol{\mu}_i(t) &= \left[x_{a,i}(t), \dot{x}_{a,i}(t), y_{a,i}(t), \dot{y}_{a,i}(t)\right]^{\mathrm{T}} \\ \boldsymbol{p}_i(t) &= \left[x_{a,i}(t), y_{a,i}(t)\right]^{\mathrm{T}} \\ \boldsymbol{u}_i(t) &= \left[u_{x,i}(t), u_{y,i}(t)\right]^{\mathrm{T}} \\ \boldsymbol{d}_i(t) &= \left[d_{1,i}(t), d_{2,i}(t)\right]^{\mathrm{T}} \\ \boldsymbol{f}_i(t) &= \boldsymbol{0} \\ \boldsymbol{A}_i &= \begin{bmatrix} 0 & 1 & 0 & 0 \\ 0 & -\zeta_{x,i}/m_{a,i} & 0 & 0 \\ 0 & 0 & 0 & 1 \\ 0 & 0 & 0 & -\zeta_{y,i}\dot{y}_{a,i}/m_{a,i} \end{bmatrix} \\ \boldsymbol{B}_i &= \boldsymbol{I}_2 \otimes \begin{bmatrix} 0 \\ 1 \end{bmatrix} \\ \boldsymbol{C}_i &= \boldsymbol{I}_2 \otimes \begin{bmatrix} 1 & 0 \end{bmatrix} \end{aligned} \tag{16}$$

Notably, the matrix B_i of each agent is a full column rank, such that there exists matrices $\mathcal{B}_{1,i} \in \mathbb{R}^{2\times 4}$ and $\mathcal{B}_{2,i} \in \mathbb{R}^{2\times 4}$ to be determined, such that $\mathcal{B}_{1,i}\boldsymbol{B}_i = \boldsymbol{I}_2$ and $\mathcal{B}_{2,i}\boldsymbol{B}_i = \boldsymbol{0}$. In addition, the matrix $\boldsymbol{\mathcal{B}}_i = \left[\mathcal{B}_{1,i}^{\mathrm{T}}, \mathcal{B}_{2,i}^{\mathrm{T}}\right]^{\mathrm{T}}$ is nonsingular. The following assumptions are helpful for the design and analysis of the TFT control protocol in USV–UAV systems.

Remark 6. The formation control model expressed in

Equation (14) is crucial for the simplification of the subsequent TFT control protocol design. Given Assumption 2 and the boundedness of the attitude of each agent, there exists an unknown upper bound $\bar{\delta}_i$ with $\left\| \boldsymbol{d}_i(t) \right\| \leqslant \bar{\delta}_i$. Based on the definition of virtual control input $\boldsymbol{u}_i(t)$, the thrust and torque of USV $i, (i = 1, 2, 3)$ can be solved as $\left[f_i, T_i \right]^{\mathrm{T}} = \boldsymbol{\Omega}_i^{-1} \boldsymbol{u}_i(t)$, and the desired attitude angles for the ith UAV $(i = 4, 5, 6, 7)$ are given as $\begin{bmatrix} \phi_{a,i}^* \\ \theta_{a,i}^* \end{bmatrix} = \begin{bmatrix} \sin\varphi_{a,i}/g & -\cos\varphi_{a,i}/g \\ \cos\varphi_{a,i}/g & \sin\varphi_{a,i}/g \end{bmatrix} \boldsymbol{u}_i(t)$.

Assumption 3. For the given time-varying formation $\boldsymbol{h}_i(t)$, the following formation-feasible condition should be met $\mathcal{B}_{2,i} \boldsymbol{X}_i \left(\boldsymbol{S}\boldsymbol{h}_i(t) - \dot{\boldsymbol{h}}_i(t) \right) = 0$.

Assumption 4. The following regulation equation has the solution pair $(\boldsymbol{X}_i, \boldsymbol{U}_i)$:

$$\begin{cases} \boldsymbol{X}_i \boldsymbol{S} = \boldsymbol{A}_i \boldsymbol{X}_i + \boldsymbol{B}_i \boldsymbol{U}_i \\ \boldsymbol{0} = \boldsymbol{C}_i \boldsymbol{X}_i - \boldsymbol{F} \end{cases} \tag{17}$$

Remark 7. Not all time-varying formation configurations can be realized by USV–UAV systems subjected to the dynamic properties. Assumption 3 restricts the desired formation configuration according to the dynamic constraints of the transformed models. In practical applications, the desired formations should be selected based on Assumption 3 for the accomplishment of TFT.

Remark 8. The solvability of the regulation equation (Equation (17)) is a precondition for TFT in this paper. Notably, Assumption 4 is a standard process for cooperative control of heterogeneous swarm systems based on output regulation (Hua et al., 2020). This regulation equation is of great significance for dealing with the heterogeneous characteristics of the USV–UAV systems and realizing TFT.

3.2 Distributed observer design

Multiple leaders exist in the swarm system, and the states of the leaders are only knowable for a part of the vehicles. However, the real-time states of all leaders are especially indispensable for the entire USV–UAV system to realize the TFT. Therefore, a distributed observer for each agent to estimate the global states of all virtual leaders is designed as follows:

$$\begin{aligned} \dot{\hat{\boldsymbol{i}}}_{i,j}(t) = \boldsymbol{S}\hat{\boldsymbol{i}}_{i,j}(t) - \vartheta_1 \sum_{k=1}^{M} w_{ik} \left(\hat{\boldsymbol{i}}_{i,j}(t) - \hat{\boldsymbol{i}}_{k,j}(t) \right) - \\ \vartheta_2 w_{ij} \boldsymbol{K} \left(\boldsymbol{F}\hat{\boldsymbol{i}}_{i,j}(t) - \boldsymbol{p}_j(t) \right) \end{aligned} \tag{18}$$

where ϑ_1 and ϑ_2 are positive constants to be determined. $\hat{\boldsymbol{i}}_{i,j}(t) \in \mathbb{R}^{n_L}$ and $\hat{\boldsymbol{i}}_{k,j}(t) \in \mathbb{R}^{n_L}$ represent the estimations of agents i and k for the states of the leader j, respectively. $\boldsymbol{p}_j(t)$ denotes the position vector of the leader, and $\boldsymbol{S}$ and $\boldsymbol{F}$ are the known constant system matrix of the leader. $\boldsymbol{K} = \boldsymbol{P}^{-1}\boldsymbol{F}^{\mathrm{T}}$ is a constant gain matrix, where $\boldsymbol{P}$ is a positive definite matrix defined by the following linear matrix inequality (LMI):

$$\boldsymbol{S}^{\mathrm{T}}\boldsymbol{P} + \boldsymbol{P}\boldsymbol{S} - \boldsymbol{F}^{\mathrm{T}}\boldsymbol{F} < 0 \tag{19}$$

Remark 9. Based on the proposed distributed observer, the problem induced by the lack of global information of the leaders is overcome effectively. Each member of the USV–UAV system can obtain the real-time states of the leaders by only using the information of the neighbors (the observed result $\hat{\boldsymbol{i}}_{k,j}(t)$) and the positions of the leaders $\boldsymbol{p}_j(t)$. Thus, the reference center can be determined through distributed communications. Notably, the gain matrix $\boldsymbol{P}$ is determined by the model of the leaders, which cannot be freely chosen. Thus, to ensure the estimation effect, the parameters of the observer also need to be discussed in the subsequent stability analysis part.

Theorem 1. If ϑ_1 and ϑ_2 are large enough, then the estimation $\hat{\boldsymbol{i}}_{i,j}(t)$ will converge to the states of the jth leader, i.e., $\lim_{t \to \infty} \left(\hat{\boldsymbol{i}}_{i,j}(t) - \boldsymbol{v}_j(t) \right) = \boldsymbol{0}$ under the distributed observer expressed in Equation (18) and Assumption 1.

Proof. Let $\hat{\boldsymbol{i}}_i(t) = \left[\hat{\boldsymbol{i}}_{i,M+1}^{\mathrm{T}}(t), \hat{\boldsymbol{i}}_{i,M+2}^{\mathrm{T}}(t), \cdots, \hat{\boldsymbol{i}}_{i,M+N}^{\mathrm{T}}(t) \right]^{\mathrm{T}}$ represent the state estimation of the agent i for all leaders. From Equation (18) and the dynamical model of the leader expressed in Equation (4), the following expression can be derived:

$$\begin{aligned} \dot{\hat{\boldsymbol{i}}}_i(t) = \left(\boldsymbol{I}_N \otimes \boldsymbol{S} \right) \hat{\boldsymbol{i}}_i(t) - \vartheta_1 \sum_{k=1}^{M} w_{ik} \left(\hat{\boldsymbol{i}}_i(t) - \hat{\boldsymbol{i}}_k(t) \right) - \\ \vartheta_2 \operatorname*{diag}_{j = M+1, M+2, \cdots, M+N} \left\{ w_{ij} \boldsymbol{P}^{-1} \boldsymbol{F}^{\mathrm{T}} \boldsymbol{F} \right\} \left(\hat{\boldsymbol{i}}_i(t) - \boldsymbol{v}_L(t) \right) \end{aligned} \tag{20}$$

The estimation error of the observer i can be defined as $\tilde{\boldsymbol{i}}_i(t) = \hat{\boldsymbol{i}}_i(t) - \boldsymbol{v}_L(t)$, where $\boldsymbol{v}_L(t) = \left[\boldsymbol{v}_{M+1}^{\mathrm{T}}(t), \boldsymbol{v}_{M+2}^{\mathrm{T}}(t), \cdots, \boldsymbol{v}_{M+N}^{\mathrm{T}}(t) \right]^{\mathrm{T}}$ is the state of virtual leaders. From Equation (20), we can obtain the following expression:

$$\begin{aligned} \dot{\tilde{\boldsymbol{i}}}_i(t) = \left(\boldsymbol{I}_N \otimes \boldsymbol{S} \right) \tilde{\boldsymbol{i}}_i(t) - \vartheta_1 \sum_{k=1}^{M} w_{ik} \left(\tilde{\boldsymbol{i}}_i(t) - \tilde{\boldsymbol{i}}_k(t) \right) - \\ \vartheta_2 \operatorname*{diag}_{j = M+1, M+2, \cdots, M+N} \left\{ w_{ij} \boldsymbol{P}^{-1} \boldsymbol{F}^{\mathrm{T}} \boldsymbol{F} \right\} \tilde{\boldsymbol{i}}_i(t) \end{aligned} \tag{21}$$

To verify the stability of the distributed observer, we consider the following differentiable candidate Lyapunov function:

$$V_{\mathrm{ob}} = \sum_{i=1}^{M} \tilde{\boldsymbol{i}}_i^{\mathrm{T}}(t) \left(\boldsymbol{I}_N \otimes \boldsymbol{P} \right) \tilde{\boldsymbol{i}}_i(t) \tag{22}$$

By inserting Equation (21), the derivative of Equation (22) can be obtained as follows:

$$\dot{V}_{\text{ob}} = \tilde{\boldsymbol{i}}^{\text{T}}(t)\left(\boldsymbol{I}_M \otimes \left(\boldsymbol{I}_N \otimes \left(\boldsymbol{S}^{\text{T}}\boldsymbol{P} + \boldsymbol{P}\boldsymbol{S}\right)\right)\right)\tilde{\boldsymbol{i}}(t) - 2\vartheta_1\tilde{\boldsymbol{i}}^{\text{T}}(t)\left(\boldsymbol{L}_F \otimes \left(\boldsymbol{I}_N \otimes \boldsymbol{P}\right)\right)\tilde{\boldsymbol{i}}(t) - 2\vartheta_2\tilde{\boldsymbol{i}}^{\text{T}}(t)\operatorname*{diag}_{i=1,2,\cdots,M}\left\{\operatorname*{diag}_{j=M+1,M+2,\cdots,M+N}\left\{w_{ij}\boldsymbol{F}^{\text{T}}\boldsymbol{F}\right\}\right\}\tilde{\boldsymbol{i}}(t) \tag{23}$$

where $\tilde{\boldsymbol{i}}(t) = \left[\tilde{\boldsymbol{i}}_1^{\text{T}}(t), \tilde{\boldsymbol{i}}_2^{\text{T}}(t), \cdots, \tilde{\boldsymbol{i}}_M^{\text{T}}(t)\right]^{\text{T}}$ is the overall estimation error. It follows from Assumption 1 and Lemma 1 that, for the follower subgraph G_F, there exists an orthogonal matrix $\boldsymbol{Q}_F = \left[\boldsymbol{1}_M/\sqrt{M}, \boldsymbol{Q}_{F,1}\right] \in \mathbb{R}^{M\times M}$ with $\boldsymbol{Q}_{F,1} \in \mathbb{R}^{M\times(M-1)}$, such that $\boldsymbol{Q}_F^{\text{T}}\boldsymbol{L}_F\boldsymbol{Q}_F = \boldsymbol{D}_F = \text{diag}\left\{0, \boldsymbol{\Lambda}_F\right\}$, where $\boldsymbol{\Lambda}_F = \text{diag}\left\{\lambda_{F,2}, \lambda_{F,3}, \cdots, \lambda_{F,M}\right\}$. Let $\tilde{\boldsymbol{\xi}}(t) = \left(\boldsymbol{Q}_F^{\text{T}} \otimes \boldsymbol{I}_{Nn_L}\right)\tilde{\boldsymbol{i}}(t)$. From Equation (23), we can further derive the following expression:

$$\dot{V}_{\text{ob}} = \tilde{\boldsymbol{\xi}}^{\text{T}}(t)\left(\boldsymbol{I}_M \otimes \left(\boldsymbol{I}_N \otimes \left(\boldsymbol{S}^{\text{T}}\boldsymbol{P} + \boldsymbol{P}\boldsymbol{S}\right)\right) - 2\vartheta_1\left(\boldsymbol{D}_F \otimes \left(\boldsymbol{I}_N \otimes \boldsymbol{P}\right)\right) - 2\vartheta_2\bar{\boldsymbol{Q}}_F^{\text{T}}\operatorname*{diag}_{i=1,2,\cdots,M}\left\{\operatorname*{diag}_{j=M+1,M+2,\cdots,M+N}\left\{w_{ij}\boldsymbol{F}^{\text{T}}\boldsymbol{F}\right\}\right\}\bar{\boldsymbol{Q}}_F\right)\tilde{\boldsymbol{\xi}}(t) \tag{24}$$

where $\bar{\boldsymbol{Q}}_F = \boldsymbol{Q}_F \otimes \boldsymbol{I}_{Nn_L}$. To facilitate, let

$$\boldsymbol{R}_{\text{ob}} = \boldsymbol{I}_M \otimes \left(\boldsymbol{I}_N \otimes \left(\boldsymbol{S}^{\text{T}}\boldsymbol{P} + \boldsymbol{P}\boldsymbol{S}\right)\right) - 2\vartheta_1\left(\boldsymbol{D}_F \otimes \left(\boldsymbol{I}_N \otimes \boldsymbol{P}\right)\right) - 2\vartheta_2\bar{\boldsymbol{Q}}_F^{\text{T}}\operatorname*{diag}_{i=1,2,\cdots,M}\left\{\operatorname*{diag}_{j=M+1,M+2,\cdots,M+N}\left\{w_{ij}\boldsymbol{F}^{\text{T}}\boldsymbol{F}\right\}\right\}\bar{\boldsymbol{Q}}_F \tag{25}$$

The expression of $\boldsymbol{R}_{\text{ob}}$ shows that it is a symmetric matrix, i. e., $\boldsymbol{R}_{\text{ob}} = \begin{bmatrix}\boldsymbol{R}_{11} & \boldsymbol{R}_{12}\\ \boldsymbol{R}_{12}^{\text{T}} & \boldsymbol{R}_{22}\end{bmatrix}$. To prove the convergence of the observer, $\boldsymbol{R}_{\text{ob}} < 0$ will be verified with the appropriate ϑ_1 and ϑ_2. According to the definition of matrix $\boldsymbol{D}_F$ and Equation (25), we can obtain the following expression:

$$\begin{aligned}
\boldsymbol{R}_{11} &= \operatorname*{diag}_{j=M+1,M+2,\cdots,M+N}\left\{\boldsymbol{S}^{\text{T}}\boldsymbol{P} + \boldsymbol{P}\boldsymbol{S} - \frac{2\vartheta_2}{M}\sum_{i=1}^{M} w_{ij}\boldsymbol{F}^{\text{T}}\boldsymbol{F}\right\}\\
\boldsymbol{R}_{12} &= -2\vartheta_2\left(\frac{\boldsymbol{1}_M^{\text{T}}}{\sqrt{M}} \otimes \boldsymbol{I}_{Nn_L}\right)\times \operatorname*{diag}_{i=1,2,\cdots,M}\left\{\operatorname*{diag}_{j=M+1,M+2,\cdots,M+N}\left\{w_{ij}\boldsymbol{F}^{\text{T}}\boldsymbol{F}\right\}\right\}\bar{\boldsymbol{Q}}_{F,1}\\
\boldsymbol{R}_{22} &= \boldsymbol{I}_{M-1} \otimes \left(\boldsymbol{I}_N \otimes \left(\boldsymbol{S}^{\text{T}}\boldsymbol{P} + \boldsymbol{P}\boldsymbol{S}\right)\right) - 2\vartheta_1\left(\boldsymbol{\Lambda}_F \otimes \left(\boldsymbol{I}_N \otimes \boldsymbol{P}\right)\right) - 2\vartheta_2\bar{\boldsymbol{Q}}_F^{\text{T}}\operatorname*{diag}_{i=1,2,\cdots,M}\left\{\operatorname*{diag}_{j=M+1,M+2,\cdots,M+N}\left\{w_{ij}\boldsymbol{F}^{\text{T}}\boldsymbol{F}\right\}\right\}\bar{\boldsymbol{Q}}_F
\end{aligned} \tag{26}$$

where $\bar{\boldsymbol{Q}}_{F,1} = \boldsymbol{Q}_{F,1} \otimes \boldsymbol{I}_{Nn_L}$. Considering the LMI (Equation (19)) and $\sum_{i=1}^{M} w_{ij} > 0$ under Assumption 1 and that ϑ_1 and ϑ_2 are large enough, we can obtain the following expression:

$$\begin{cases}\boldsymbol{R}_{11} < 0\\ \boldsymbol{R}_{22} - \boldsymbol{R}_{12}^{\text{T}}\boldsymbol{R}_{11}^{-1}\boldsymbol{R}_{12} = \boldsymbol{\Phi} - 2\vartheta_1\left(\boldsymbol{\Lambda}_F \otimes \left(\boldsymbol{I}_N \otimes \boldsymbol{P}\right)\right) < 0\end{cases} \tag{27}$$

Based on Lemma 2, $\boldsymbol{R}_{\text{ob}} < 0$ can be obtained. Therefore, $\dot{V}_{\text{ob}} \leqslant 0$ can be verified. Moreover, it follows from Equation (24) that $\tilde{\boldsymbol{i}}(t) = \boldsymbol{0}$ when $\dot{V}_{\text{ob}} = 0$. From LaSalle's invariance principle, $\lim_{t\to\infty}\tilde{\boldsymbol{i}}_i(t) = \lim_{t\to\infty}\left(\hat{\boldsymbol{i}}_i(t) - \boldsymbol{v}_L(t)\right) = \boldsymbol{0}$ can be obtained.

This completes the proof of Theorem 1.

Remark 10. According to the previously presented analysis, some rules of the parameter setting strategy for DETO can be summarized as follows: For the observation system, the convergence property of $\tilde{\boldsymbol{i}}_i(t)$ is determined using ϑ_1 and ϑ_2, where larger parameters guarantee a more effective estimation. Based on Equation (26), the inequality expressed in Equation (27) is satisfied in the case where $\vartheta_2 > M\Big/\left(2\min_{j=M+1,M+2,\cdots,M+N}\sum_{i=1}^{M} w_{ij}\right)$ and $\vartheta_1 > \max\left\{0, \frac{\lambda_{\max}(\boldsymbol{\Phi})}{2\lambda_{\min}(\boldsymbol{\Lambda}_F)\lambda_{\min}(\boldsymbol{P})}\right\}$, where

$$\boldsymbol{\Phi} = \boldsymbol{I}_{M-1} \otimes \left(\boldsymbol{I}_N \otimes \left(\boldsymbol{S}^{\text{T}}\boldsymbol{P} + \boldsymbol{P}\boldsymbol{S}\right)\right) - 2\vartheta_2\bar{\boldsymbol{Q}}_{F,1}^{\text{T}}\operatorname*{diag}_{i=1,2,\cdots,M}\left\{\operatorname*{diag}_{j=M+1,M+2,\cdots,M+N}\left\{w_{ij}\boldsymbol{F}^{\text{T}}\boldsymbol{F}\right\}\right\}\bar{\boldsymbol{Q}}_{F,1} - \boldsymbol{R}_{12}^{\text{T}}\boldsymbol{R}_{11}^{-1}\boldsymbol{R}_{12} \tag{28}$$

Therefore, the parameters should be selected reasonably.

3.3 Adaptive TFT regulation control protocol design

We consider a USV–UAV system consisting of n_s USVs and $M - n_s$ UAVs that suffers from bounded unknown external disturbances. To tackle the issue of USV−UAV TFT, the following error definition is given.

Definition 1. The formation state tracking error of the follower i can be described as follows:

$$\boldsymbol{e}_i(t) = \boldsymbol{\mu}_i(t) - \boldsymbol{X}_i\left(\sum_{j=M+1}^{M+N}\rho_j\boldsymbol{v}_j(t) + \boldsymbol{h}_i(t)\right) \tag{29}$$

where $\sum_{j=M+1}^{M+N}\rho_j\boldsymbol{v}_j(t)$ represents the expected formation reference center state generated by multiple leaders, and $\boldsymbol{h}_i(t)$ is the expected time-varying formation vector that satisfies

Assumption 3. Based on Equation (14) and the regulation equation (Equation (17)), we obtain $\boldsymbol{C}_i\boldsymbol{e}_i(t)=\boldsymbol{p}_i(t)-\boldsymbol{\Delta}_i(t)-\mathcal{P}_L(t)$, such that the convergence of $\boldsymbol{e}_i(t)$ is equivalent to the realization of time-varying formations.

By resorting to Lemma 3, the nonlinear uncertain term $\boldsymbol{f}_i(t)$ and the bounded disturbance $\boldsymbol{d}_i(t)$ in Equation (14) can be approximated as $\boldsymbol{f}_i(t)+\boldsymbol{d}_i(t)=\boldsymbol{W}_i^{\mathrm{T}}\boldsymbol{G}_i+\boldsymbol{\varepsilon}_i$. According to the MLP algorithm, we obtain $\left\|\boldsymbol{f}_i(t)+\boldsymbol{d}_i(t)\right\|\leqslant\Gamma_i\gamma_i(\boldsymbol{x})+R_i$, where $\gamma(\boldsymbol{x})=\left\|\mathcal{G}(\boldsymbol{x})\right\|$ denotes the output vector norm of the hidden layer. In this way, the computational load and the difficulty of subsequent stability analysis are considerably reduced. Then, the adaptive TFT regulation control protocol for the follower i is designed as follows:

$$\boldsymbol{u}_i(t)=\boldsymbol{K}_{1,i}\boldsymbol{\mu}_i(t)+\boldsymbol{K}_{2,i}\left(\sum_{j=M+1}^{M+N}\rho_j\hat{\boldsymbol{\imath}}_{i,j}(t)+\boldsymbol{h}_i(t)\right)-\boldsymbol{r}_{h,i}(t)-\boldsymbol{r}_{f,i}(t) \tag{30}$$

with

$$\boldsymbol{r}_{h,i}(t)=\mathfrak{B}_{1,i}\boldsymbol{X}_i\left(\boldsymbol{S}\boldsymbol{h}_i(t)-\dot{\boldsymbol{h}}_i(t)\right) \tag{31}$$

$$\boldsymbol{r}_{f,i}=\frac{\left(\hat{\Gamma}_i\gamma_i\right)^2\boldsymbol{B}_i^{\mathrm{T}}\boldsymbol{e}_i(t)}{\hat{\Gamma}_i\gamma_i\left\|\boldsymbol{B}_i^{\mathrm{T}}\boldsymbol{e}_i(t)\right\|+c_{1,i}}+\frac{\hat{R}_i^2\boldsymbol{B}_i^{\mathrm{T}}\boldsymbol{e}_i(t)}{\hat{R}_i\left\|\boldsymbol{B}_i^{\mathrm{T}}\boldsymbol{e}_i(t)\right\|+c_{2,i}} \tag{32}$$

where $c_{1,i}$ and $c_{2,i}$ are positive design parameters, and $\boldsymbol{K}_{1,i}$ and $\boldsymbol{K}_{2,i}=\boldsymbol{U}_i-\boldsymbol{K}_{1,i}\boldsymbol{X}_i$ are the gain constant matrices. Furthermore, $\hat{\Gamma}_i$ and $\hat{R}_i$ represent the adaptive estimations for the parameters Γ_i and R_i of the MLP-based RBFNN.

Inspired by Bounemeur et al. (2018), the adaptive update laws are designed as follows:

$$\dot{\hat{\Gamma}}_i=-k_{1,i}c_{1,i}\hat{\Gamma}_i+k_{1,i}\gamma_i\left\|\boldsymbol{B}_i^{\mathrm{T}}\boldsymbol{e}_i(t)\right\| \tag{33}$$

$$\dot{\hat{R}}_i=-k_{2,i}c_{2,i}\hat{R}_i+k_{2,i}\left\|\boldsymbol{B}_i^{\mathrm{T}}\boldsymbol{e}_i(t)\right\| \tag{34}$$

where $k_{1,i}$, $k_{2,i}$, $c_{2,i}$, and $c_{2,i}$ denote positive constants to be determined. The initial values of these adaptive parameters are limited to $\hat{\Gamma}_i(t_0)>0$ and $\hat{R}_i(t_0)>0$.

3.4 Stability analysis

In this subsection, the following theorem guarantees that the time-varying formation can be realized by the USV–UAV systems under the presented scheme.

Theorem 2. We consider a USV–UAV system with n_s USVs and $M-n_s$ UAVs that suffers from time-varying formation and bounded external disturbances under Assumption 2. If Assumption 1 holds and the time-varying formation $\boldsymbol{h}_i(t)$ satisfies Assumption 3, the virtual control input is generated by the control scheme expressed in Equation (30). Moreover, $\boldsymbol{K}_{1,i}$ should be designed to ensure that $\boldsymbol{A}_i+\boldsymbol{B}_i\boldsymbol{K}_{1,i}$ is Hurwitz and the parameters of the adaptive update laws meet $\max\left\{c_{1,i}k_{1,i},c_{2,i}k_{2,i}\right\}\leqslant-2\lambda_{\max}\left(\boldsymbol{A}_i+\boldsymbol{B}_i\boldsymbol{K}_{1,i}\right)$. Then, the control objective could be achieved.

Proof. To show the stability of the agent i within the USV–UAV system, the candidate Lyapunov function is selected as follows:

$$V_i=\frac{1}{2}\boldsymbol{e}_i^{\mathrm{T}}(t)\boldsymbol{e}_i(t)+\frac{1}{2k_{1,i}}\tilde{\Gamma}_i^2+\frac{1}{2k_{2,i}}\tilde{R}_i^2 \tag{35}$$

where $\tilde{\Gamma}_i=\Gamma_i-\hat{\Gamma}_i$ and $\tilde{R}_i=R_i-\hat{R}_i$ are the adaptive estimation errors. By substituting the control protocol into the like-linear model, the tracking error system can be transformed into the following expression:

$$\begin{aligned}\dot{\boldsymbol{e}}_i(t)=&\left(\boldsymbol{A}_i+\boldsymbol{B}_i\boldsymbol{K}_{1,i}\right)\boldsymbol{e}_i(t)+\\&\left(\boldsymbol{A}_i+\boldsymbol{B}_i\boldsymbol{K}_{1,i}\right)\boldsymbol{X}_i\left(\sum_{j=M+1}^{M+N}\rho_j\boldsymbol{v}_j(t)+\boldsymbol{h}_i(t)\right)+\\&\boldsymbol{B}_i\boldsymbol{K}_{2,i}\left(\sum_{j=M+1}^{M+N}\rho_j\hat{\boldsymbol{\imath}}_{i,j}(t)+\boldsymbol{h}_i(t)\right)-\\&\boldsymbol{B}_i\boldsymbol{r}_{h,i}(t)+\boldsymbol{B}_i\left(\boldsymbol{f}_i(t)+\boldsymbol{d}_i(t)-\boldsymbol{r}_{f,i}(t)\right)-\\&\boldsymbol{X}_i\left(\sum_{j=M+1}^{M+N}\rho_j\dot{\boldsymbol{v}}_j(t)+\dot{\boldsymbol{h}}_i(t)\right)\end{aligned} \tag{36}$$

Given that $\boldsymbol{K}_{2,i}=\boldsymbol{U}_i-\boldsymbol{K}_{1,i}\boldsymbol{X}_i$ and $\boldsymbol{\imath}(t)$ satisfied $\dot{\boldsymbol{\imath}}(t)=\boldsymbol{S}\boldsymbol{\imath}(t)$, recalling Equation (17) yields the following expression:

$$\begin{aligned}\dot{\boldsymbol{e}}_i(t)=&\left(\boldsymbol{A}_i+\boldsymbol{B}_i\boldsymbol{K}_{1,i}\right)\boldsymbol{e}_i(t)+\boldsymbol{X}_i\boldsymbol{S}\boldsymbol{h}_i(t)-\boldsymbol{X}_i\dot{\boldsymbol{h}}_i(t)-\\&\boldsymbol{B}_i\boldsymbol{r}_{h,i}(t)+\boldsymbol{B}_i\left(\boldsymbol{f}_i(t)+\boldsymbol{d}_i(t)-\boldsymbol{r}_{f,i}(t)\right)+\\&\boldsymbol{B}_i\boldsymbol{K}_{2,i}\sum_{j=M+1}^{M+N}\rho_j\tilde{\boldsymbol{\imath}}_{i,j}(t)\end{aligned} \tag{37}$$

Given that $\mathfrak{B}_{1,i}\boldsymbol{B}_i=\boldsymbol{I}_2$, $\mathfrak{B}_{2,i}\boldsymbol{B}_i=\boldsymbol{0}$, and the time-varying formation obeys Assumption 3, we obtain the following expression:

$$\mathfrak{B}_{2,i}\boldsymbol{X}_i\left(\boldsymbol{S}\boldsymbol{h}_i(t)-\dot{\boldsymbol{h}}_i(t)\right)-\mathfrak{B}_{2,i}\boldsymbol{B}_i\boldsymbol{r}_{h,i}(t)=\boldsymbol{0} \tag{38}$$

Based on the definition of the time-varying formation compensation $\boldsymbol{r}_{h,i}(t)$, it holds the following:

$$\mathfrak{B}_{1,i}\boldsymbol{X}_i\left(\boldsymbol{S}\boldsymbol{h}_i(t)-\dot{\boldsymbol{h}}_i(t)\right)-\mathfrak{B}_{1,i}\boldsymbol{B}_i\boldsymbol{r}_{h,i}(t)=\boldsymbol{0} \tag{39}$$

As $\boldsymbol{\mathfrak{B}}_i=\left[\mathfrak{B}_{1,i}^{\mathrm{T}},\mathfrak{B}_{2,i}^{\mathrm{T}}\right]^{\mathrm{T}}$ is nonsingular, it holds from Equa-

tions (38) and (39) the following:

$$\boldsymbol{X}_i\boldsymbol{S}\boldsymbol{h}_i(t) - \boldsymbol{X}_i\dot{\boldsymbol{h}}_i(t) - \boldsymbol{B}_i\boldsymbol{r}_{h,i}(t) = \boldsymbol{0} \tag{40}$$

Moreover, if Theorem 1 holds, Equation (37) can be further expressed as follows:

$$\dot{\boldsymbol{e}}_i(t) = \left(\boldsymbol{A}_i + \boldsymbol{B}_i\boldsymbol{K}_{1,i}\right)\boldsymbol{e}_i(t) + \boldsymbol{B}_i\left(\boldsymbol{f}_i(t) + \boldsymbol{d}_i(t) - \boldsymbol{r}_{f,i}(t)\right) \tag{41}$$

We take the time derivative of V_i as follows:

$$\begin{aligned}\dot{V}_i = {} & \frac{1}{2}\boldsymbol{e}_i^{\mathrm{T}}(t)\left[\left(\boldsymbol{A}_i + \boldsymbol{B}_i\boldsymbol{K}_{1,i}\right) + \left(\boldsymbol{A}_i + \boldsymbol{B}_i\boldsymbol{K}_{1,i}\right)^{\mathrm{T}}\right]\boldsymbol{e}_i(t) + \\ & \boldsymbol{e}_i^{\mathrm{T}}\boldsymbol{B}_i\left(\boldsymbol{f}_i(t) + \boldsymbol{d}_i(t) - \boldsymbol{r}_{f,i}(t)\right) + \\ & \frac{1}{k_{1,i}}\tilde{\Gamma}_i\dot{\tilde{\Gamma}}_i + \frac{1}{k_{2,i}}\tilde{R}_i\dot{\tilde{R}}_i\end{aligned} \tag{42}$$

where the matrix $\boldsymbol{A}_i + \boldsymbol{B}_i\boldsymbol{K}_{1,i}$ is ensured to be Hurwitz, depending on $\boldsymbol{K}_{1,i}$, which indicates that all eigenvalues of $\boldsymbol{A}_i + \boldsymbol{B}_i\boldsymbol{K}_{1,i}$ have negative real parts. Based on the MLP-based RBFNN method, if the inequality $\boldsymbol{e}_i^{\mathrm{T}}(t)\boldsymbol{B}_i\left(\boldsymbol{f}_i(t) + \boldsymbol{d}_i(t)\right) \leqslant \left\|\boldsymbol{B}_i^{\mathrm{T}}\boldsymbol{e}_i(t)\right\|\left(\bar{\Gamma}_i\gamma_i + \bar{R}_i\right)$ holds, then the following inequality can be derived:

$$\begin{aligned}\dot{V}_i \leqslant {} & \lambda_{\max}\left(\boldsymbol{A}_i + \boldsymbol{B}_i\boldsymbol{K}_{1,i}\right)\boldsymbol{e}_i^{\mathrm{T}}(t)\boldsymbol{e}_i(t) + \left\|\boldsymbol{B}_i^{\mathrm{T}}\boldsymbol{e}_i(t)\right\|\left(\bar{\Gamma}_i\gamma_i + \bar{R}_i\right) - \\ & \boldsymbol{e}_i^{\mathrm{T}}(t)\boldsymbol{B}_i\left(\frac{\left(\hat{\Gamma}_i\gamma_i\right)^2\boldsymbol{B}_i^{\mathrm{T}}\boldsymbol{e}_i(t)}{\hat{\Gamma}_i\gamma_i\left\|\boldsymbol{B}_i^{\mathrm{T}}\boldsymbol{e}_i(t)\right\| + c_{1,i}} + \frac{\hat{R}_i^2\boldsymbol{B}_i^{\mathrm{T}}\boldsymbol{e}_i(t)}{\hat{R}_i\left\|\boldsymbol{B}_i^{\mathrm{T}}\boldsymbol{e}_i(t)\right\| + c_{2,i}}\right) - \\ & \frac{1}{k_{1,i}}\tilde{\Gamma}_i\left(-k_{1,i}c_{1,i}\hat{\Gamma}_i + k_{1,i}\gamma_i\left\|\boldsymbol{B}_i^{\mathrm{T}}\boldsymbol{e}_i(t)\right\|\right) - \\ & \frac{1}{k_{2,i}}\tilde{R}_i\left(-k_{2,i}c_{2,i}\hat{R}_i + k_{2,i}\left\|\boldsymbol{B}_i^{\mathrm{T}}\boldsymbol{e}_i(t)\right\|\right)\end{aligned} \tag{43}$$

Based on the definition of $\tilde{\Gamma}_i$ and $\tilde{R}_i$, we first derive the following expression:

$$\begin{aligned}\dot{V}_i \leqslant {} & \lambda_{\max}\left(\boldsymbol{A}_i + \boldsymbol{B}_i\boldsymbol{K}_{1,i}\right)\boldsymbol{e}_i^{\mathrm{T}}(t)\boldsymbol{e}_i(t) + \\ & c_{1,i}\tilde{\Gamma}_i\hat{\Gamma}_i + \frac{c_{1,i}\hat{\Gamma}_i\gamma_i\left\|\boldsymbol{B}_i^{\mathrm{T}}\boldsymbol{e}_i(t)\right\|}{\hat{\Gamma}_i\gamma_i\left\|\boldsymbol{B}_i^{\mathrm{T}}\boldsymbol{e}_i(t)\right\| + c_{1,i}} + \\ & c_{2,i}\tilde{R}_i\hat{R}_i + \frac{c_{2,i}\hat{R}_i\left\|\boldsymbol{B}_i{}^{\mathrm{T}}\boldsymbol{e}_i(t)\right\|}{\hat{R}_i\left\|\boldsymbol{B}_i^{\mathrm{T}}\mathbf{e}_i(t)\right\| + c_{2,i}}\end{aligned} \tag{44}$$

and then obtain the following expression:

$$\begin{aligned}\dot{V}_i \leqslant {} & \lambda_{\max}\left(\boldsymbol{A}_i + \boldsymbol{B}_i\boldsymbol{K}_{1,i}\right)\boldsymbol{e}_i^{\mathrm{T}}(t)\boldsymbol{e}_i(t) + \\ & c_{1,i}\tilde{\Gamma}_i\hat{\Gamma}_i + c_{2,i}\tilde{R}_i\hat{R}_i + c_{1,i} + c_{2,i}\end{aligned} \tag{45}$$

According to Young's inequality, it holds the following:

$$\begin{aligned}\dot{V}_i \leqslant {} & -a_iV_i + \left(\lambda_{\max}\left(\boldsymbol{A}_i + \boldsymbol{B}_i\boldsymbol{K}_{1,i}\right) + \frac{a_i}{2}\right)\boldsymbol{e}_i^{\mathrm{T}}(t)\boldsymbol{e}_i(t) + \\ & \left(\frac{a_i}{2k_{1,i}} - \frac{c_{1,i}}{2}\right)\tilde{\Gamma}_i^2 + \left(\frac{a_i}{2k_{2,i}} - \frac{c_{2,i}}{2}\right)\tilde{R}_i^2 + \\ & \left(1 + \frac{\bar{\Gamma}_i^2}{2}\right)c_{1,i} + \left(1 + \frac{\bar{R}_i^2}{2}\right)c_{2,i}\end{aligned} \tag{46}$$

where a_i indicates a bounded positive constant with $a_i \leqslant \min\left\{c_{1,i}k_{1,i}, c_{2,i}k_{2,i}\right\}$. According to the settings for $c_{1,i}$ and $c_{2,i}$ in Theorem 2, we eventually derive the following expression:

$$\dot{V}_i \leqslant -a_iV_i - \left(-\lambda_{\max}\left(\boldsymbol{A}_i + \boldsymbol{B}_i\boldsymbol{K}_{1,i}\right) - \frac{a_i}{2}\right)\boldsymbol{e}_i^{\mathrm{T}}(t)\boldsymbol{e}_i(t) + \Theta_i \tag{47}$$

where $\Theta_i = \left(1 + \bar{\Gamma}_i^2/2\right)c_{1,i} + \left(1 + \bar{R}_i^2/2\right)c_{2,i}$. To facilitate, let

$$J_{\min,i} = -\lambda_{\max}\left(\boldsymbol{A}_i + \boldsymbol{B}_i\boldsymbol{K}_{1,i}\right) - \frac{a_i}{2} \tag{48}$$

When $\left\|\boldsymbol{e}_i(t)\right\|^2 > \Theta_i/J_{\min,i}$, the derivative of V_i yields $\dot{V}_i \leqslant -a_iV_i$. Thus, $\left\|\boldsymbol{e}_i(t)\right\|^2$ will converge to the upper bound $\Theta_i/J_{\min,i}$. Given that $\boldsymbol{p}_i(t) - \boldsymbol{\Delta}_i(t) - \mathcal{P}_L(t) = \boldsymbol{C}_i\boldsymbol{e}_i(t)$, from the definition of the matrix $\boldsymbol{C}_i$ in the USV–UAV system, the formation position error will converge to the upper bound $\mathcal{Q}_i \leqslant \Theta_i/J_{\min,i}$.

This completes the proof of Theorem 2.

Remark 11. In practical application, $c_{1,i}$, $c_{2,i}$, and $c_{3,i}$ can be reasonably chosen to ensure that the error $\boldsymbol{p}_i(t) - \boldsymbol{\Delta}_i(t) - \mathcal{P}_L(t)$ is as small as possible. If the formation error is small enough to meet practical requirements, then the TFT can be said to be accomplished by the USV–UAV system. In addition, we observe from Equation (47) that the convergence rate of $V(t)$ is mainly decided by a_i. It is possible to select design parameters on the basis of satisfying $\max\left\{c_{1,i}k_{1,i}, c_{2,i}k_{2,i}\right\} \leqslant -2\lambda_{\max}\left(\boldsymbol{A}_i + \boldsymbol{B}_i\boldsymbol{K}_{1,i}\right)$ to increase a_i and achieve faster convergence. Note that extremely small $k_{1,i}$ and $k_{2,i}$ may cause the slow convergence of the adaptive parameters. Thus, it is necessary to make a trade-off when choosing the parameters.

4 Numerical simulation

To demonstrate the effectiveness of the proposed adaptive TFT regulation controller, the TFT maneuver simulation examples are constructed according to the escort mis-

sion in this section.

A system with three USVs marked as 1–3, four quadrotor UAVs marked as 4–7, and two virtual leaders marked as 8 and 9 is considered. The nonlinear kinematic and dynamic parameters of each USV and UAV are given in Table 1 (Huang et al., 2024; Song et al., 2018). Simultaneously, the underlying communication topology is shown in Figure 3. From the reality of mission facts, only the first USV can obtain position data from two virtual leaders.

Table 1 Model parameters of the USV and UAV

Component	Value
Model parameters of the USV	$m_{11,i}=25.8, m_{22,i}=33.8, m_{33,i}=2.76,$ $d_{11,i}=0.72+1.33\lvert u_{s,i}\rvert,$ $d_{22,i}=0.889\,6+36.5\lvert v_{s,i}\rvert+0.805\lvert r_{s,i}\rvert,$ $d_{33,i}=1.9-0.08\lvert v_{s,i}\rvert+0.75\lvert r_{s,i}\rvert$
Model parameters of the UAV	$m_{a,i}=2.0, \mathrm{g}=9.8,$ $I_{x,i}=1.25, I_{y,i}=1.25, I_{z,i}=2.5,$ $\zeta_{x,i}=1.2, \zeta_{y,i}=1.2, \zeta_{z,i}=1.2,$ $\zeta_{\phi,i}=0, \zeta_{\theta,i}=0, \zeta_{\varphi,i}=0$

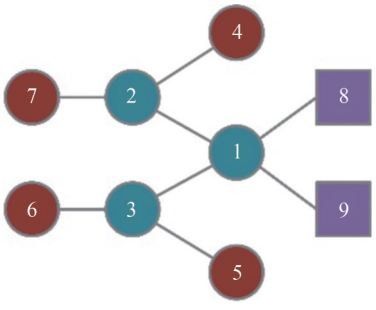


Figure 3 Interaction topology of the USV–UAV system

The external disturbances of the USVs $(i=1,2,3)$ are expressed as follows:

$$\begin{cases} d_{x,i}=9.8\sin\left(2t+(i-1)\pi/3\right)- \\ \qquad 6.2\cos\left(1.1t+(i-1)\pi/3\right)\sin(0.38t) \\ d_{y,i}=-8.8\sin\left(1.6t+(i-1)\pi/3\right)\cos\left(1.25t+(i-1)\pi/3\right)+ \\ \qquad 4.8\cos(0.55t) \\ d_{\varphi,i}=10.3\cos\left(1.2t+(i-1)\pi/3\right)\cos(0.83t)- \\ \qquad 5.2\sin(0.11t) \end{cases}$$

For the UAVs $(i=4,5,6,7)$, this paper only considers the disturbances in positioning the outer loop as follows:

$$\begin{cases} d_{1,i}=-3.25\sin\left(2t+(i-4)\pi/4\right)+3.5\cos^2(1.1t) \\ d_{2,i}=3.6\cos\left(2t+(i-4)\pi/4\right)- \\ \qquad 3.35\sin\left(1.4t+(i-4)\pi/4\right)\cos\left(0.95t+(i-4)\pi/4\right) \end{cases}$$

The USV model transformation parameter is chosen as $l_i=0.2$. In addition, the RBFNN with 64 neurons is applied to approximate the unknown terms, and the parameters of the Gaussian function are chosen as $\boldsymbol{c}=[\text{linspace}(-5,5,64)\ \text{linspace}(-5,5,64),\ \text{linspace}(-5,5,64),\ \text{linspace}(-5,5,64)]^{\mathrm{T}}$, and $\ell_j=0.8, (j=1,\cdots,64)$. Moreover, the parameters of the adaptive laws in Equations (33) and (34) are set as $k_{1,i}=10$, $k_{2,i}=1$, $c_{1,i}=0.05$, and $c_{2,i}=0.05\,(i=1,2,3,4,5,6,7)$. Meanwhile, the gain $\boldsymbol{K}_{1,i}$ can be solved by the pole assignment method to ensure that $\boldsymbol{A}_i+\boldsymbol{B}_i\boldsymbol{K}_{1,i}$ is Hurwitz and $\boldsymbol{K}_{2,i}=\boldsymbol{U}_i-\boldsymbol{K}_{1,i}\boldsymbol{X}_i$. To satisfy the constraints for the parameters discussed in Theorem 1, $\boldsymbol{A}_i+\boldsymbol{B}_i\boldsymbol{K}_{1,i}$ is plotted as $[-3.998,-3.999,-4.001,-4.002]^{\mathrm{T}}$. In addition, we choose $\rho_8=\rho_9=1/2$, which indicates that the formation reference center is defined as $\left(\boldsymbol{p}_8(t)+\boldsymbol{p}_9(t)\right)/2$. The gain parameters of the distributed observer $i\,(i=1,2,\cdots,7)$ are set as $\vartheta_1=10$ and $\vartheta_2=10$. In this section, the initial position vectors of USVs are given as $\boldsymbol{\eta}_{s,1}(0)=[3,3,0]^{\mathrm{T}}$, $\boldsymbol{\eta}_{s,2}(0)=[-3,3,0]^{\mathrm{T}}$, and $\boldsymbol{\eta}_{s,3}(0)=[3,-3,0]^{\mathrm{T}}$. We assume that UAVs 4 and 5 launch from the 1th USV, whereas UAVs 6 and 7 take off from USVs 2 and 3, respectively. The initial velocities of each vehicle are all set to zero. The initial value of the distributed observer $\hat{\boldsymbol{i}}_i(0)$ is set to the origin.

4.1 Effectiveness validation

This subsection presents the simulation of the proposed adaptive TFT for the USV–UAV systems. We assume that the leaders have the dynamic model parameters $\boldsymbol{S}=\boldsymbol{I}_2\otimes\begin{bmatrix}0 & 0.05\\ -0.05 & 0\end{bmatrix}$ and $\boldsymbol{F}=\boldsymbol{I}_2\otimes[\,1\quad 0\,]$. According to the regulation equation (Equation (17)) in Assumption 4, we can solve $\boldsymbol{X}_i=\boldsymbol{I}_2\otimes\begin{bmatrix}1 & 0\\ 0 & 0.05\end{bmatrix}(i=1,2,3,4,5,6,7)$, $\boldsymbol{U}_i=\boldsymbol{I}_2\otimes[-0.002\,5\quad 0]\,(i=1,2,3)$, and $\boldsymbol{U}_i=\boldsymbol{I}_2\otimes[-0.002\,5\quad 0.03]\,(i=4,5,6,7)$. Based on Assumption 3, the expected time-varying formations are set as follows:

$$\boldsymbol{h}_i(t)=\begin{bmatrix}4\cos\left(0.05t+(i-1)\pi/3+\pi/2\right)\\ -4\sin\left(0.05t+(i-1)\pi/3+\pi/2\right)\\ 4\sin\left(0.05t+(i-1)\pi/3+\pi/2\right)\\ 4\cos\left(0.05t+(i-1)\pi/3+\pi/2\right)\end{bmatrix},(i=1,2,3)$$

$$\boldsymbol{h}_i(t)=\begin{bmatrix}8\cos\left(0.05t+(2i-7)\pi/3\right)\\ -8\sin\left(0.05t+(2i-7)\pi/3\right)\\ 8\sin\left(0.05t+(2i-7)\pi/3\right)\\ 8\cos\left(0.05t+(2i-7)\pi/3\right)\end{bmatrix},(i=4,5,6,7)$$

The results of the simulation under the proposed TFT control scheme are shown in Figures 4–6. The trajectories from two perspectives of the system are shown in Figure 4, from which we can observe that TFT control can be achieved under the algorithm proposed in this article. The adaptability of the entire swarm to a time-varying formation is verified. Figure 5 presents the time responses of formation tracking errors. A further observation of Figures 4 and 5 indicates that the adaptive regulation control scheme effectively causes the formation tracking error to converge to a small region around zero. The adaptive estimations for Γ_i and R_i are depicted in Figure 6(a). By observing these results, we can determine that the boundedness of the adaptive parameters is guaranteed. The estimation errors of the distributed observer are given in Figure 6(b), where we observe that the estimation can converge to the states of the leaders. From the aforementioned results, we determine that the proposed TFT strategy for the USV–UAV system has satisfactory performance and robustness.

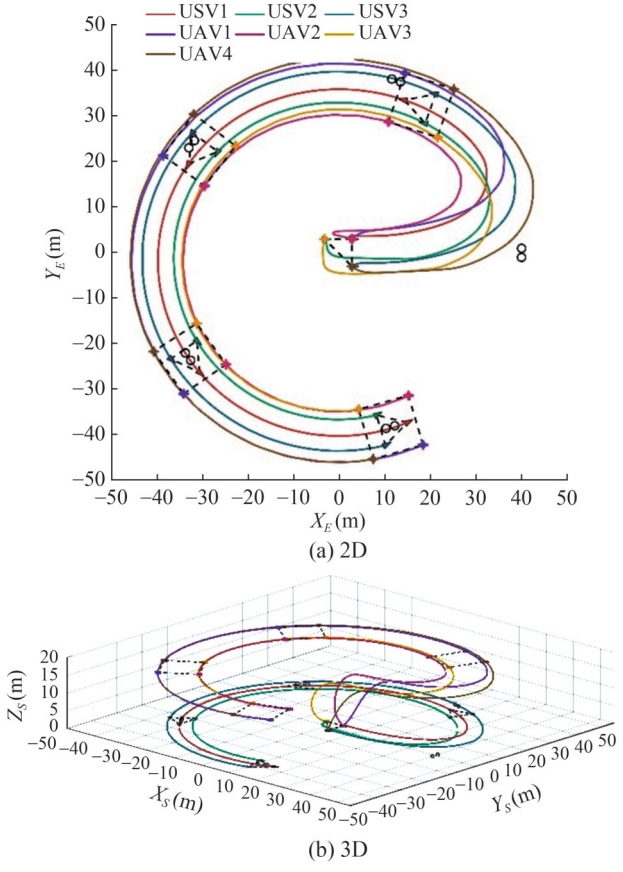


Figure 4 Trajectory in 2D and 3D space evolution of the USV–UAV system

4.2 Comparison results

In this section, the comparison results are presented to show the advantages of the proposed TFT control scheme

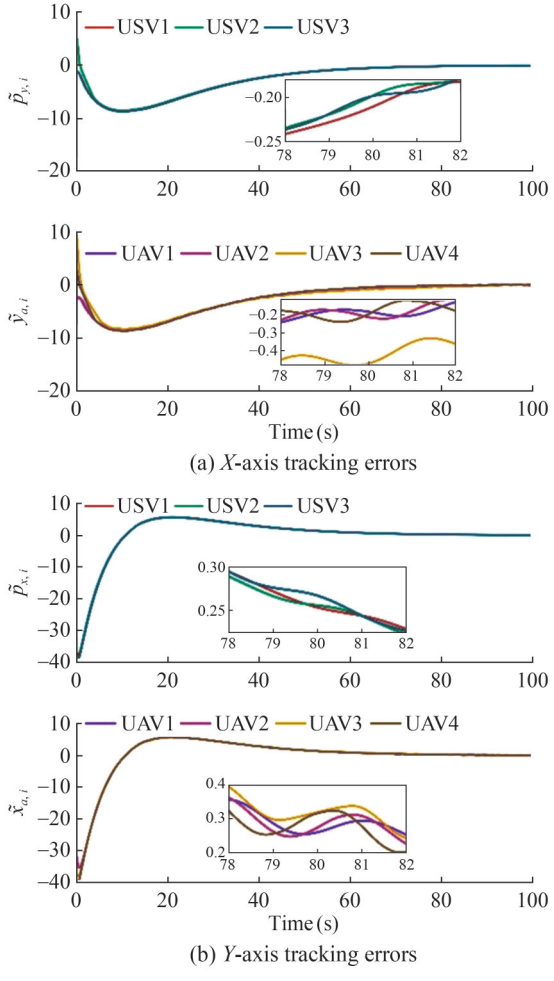
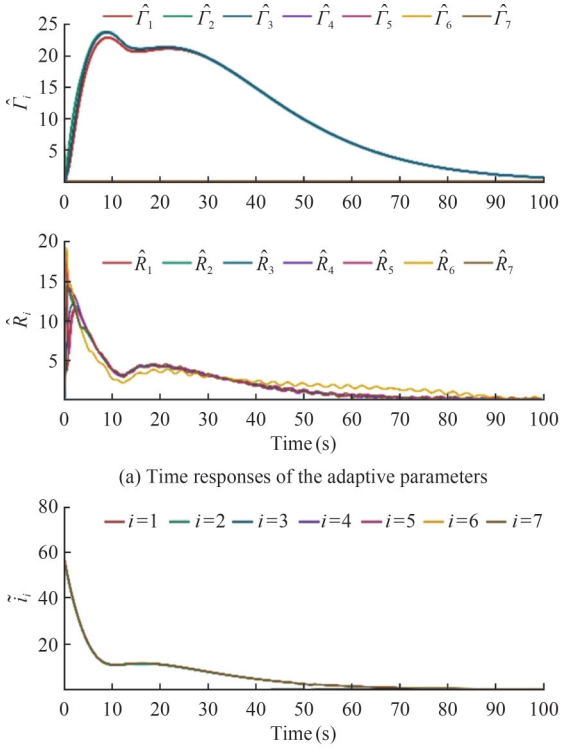


Figure 5 Time responses of formation tracking errors related to positions

(PTFTC). The leaders are modeled as $\boldsymbol{S} = \boldsymbol{I}_2 \otimes \begin{bmatrix} 0 & 1 \\ 0 & 0 \end{bmatrix}$ and $\boldsymbol{F} = \boldsymbol{I}_2 \otimes [\,1 \quad 0\,]$, and the regulation matrices are solved as $\boldsymbol{X}_i = \boldsymbol{I}_4 \,(i = 1, 2, 3, 4, 5, 6, 7)$, $\boldsymbol{U}_i = \boldsymbol{I}_2 \otimes [\,0 \quad 0\,]$ $(i = 1, 2, 3)$, and $\boldsymbol{U}_i = \boldsymbol{I}_2 \otimes [\,1 \quad 1\,]\,(i = 4, 5, 6, 7)$. Meanwhile, the desired time-varying formation satisfying Assumption 3 is obtained as follows:

$$\boldsymbol{h}_i(t) = \begin{bmatrix} 5\cos\left(2(i-1)\pi/3 + \pi/6\right) \\ 0 \\ 5\sin\left(2(i-1)\pi/3 + \pi/6\right) \\ 0 \end{bmatrix}, (i = 1, 2, 3)$$

$$\boldsymbol{h}_i(t) = \begin{bmatrix} 10\cos\left(t/8 + (i-5)\pi/2\right) \\ -10/8\sin\left(t/8 + (i-5)\pi/2\right) \\ 10\sin\left(t/8 + (i-5)\pi/2\right) \\ 10/8\cos\left(t/8 + (i-5)\pi/2\right) \end{bmatrix}, (i = 4, 5, 6, 7)$$



(a) Time responses of the adaptive parameters

(b) The estimation errors of the states of the leaders

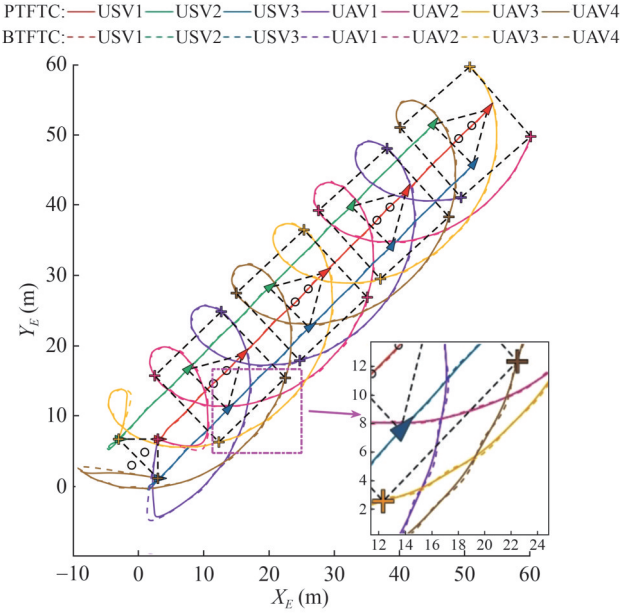
Figure 6 Time responses of the adaptive parameters and the estimation errors of the states of the leaders

We present the comparison results of the basic regulation TFT control (BTFTC) derived from the output regulation control methods (Dong and Hu, 2017). To apply the TFT protocol for linear heterogeneous systems to USV–UAV systems, the display linearization method is introduced. Specifically,

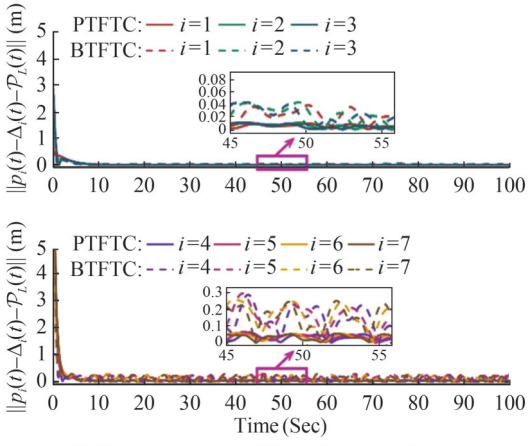
$$\boldsymbol{u}_i(t) = \boldsymbol{K}_{1,i}\boldsymbol{\mu}_i(t) + \boldsymbol{K}_{2,i}\left(\sum_{j=M+1}^{M+N}\rho_j\hat{\boldsymbol{i}}_{i,j}(t) + \boldsymbol{h}_i(t)\right) - \boldsymbol{r}_{h,i}(t) - \boldsymbol{f}_i(t) \tag{49}$$

where $\boldsymbol{f}_i(t)$ is a nonlinear term in the system expressed in Equation (14). The control gains are set to the same as those of PTFTC. The comparison of the simulation results are shown in Figure 7.

From the horizontal plane trajectories in Figure 7(a), we observe that both control schemes can achieve the TFT of the USV–UAV system. The magnified inset in Figure 7(a) illustrates that PTFTC is actively striving to alleviate chattering induced by environmental disturbances. Figure 7(b) shows the formation position error norms of each vehicle. Obviously, PTFTC achieved better control effect compared to BTFTC, with fewer shakes and tracking errors, indicating that the proposed scheme preserves satisfactory control performance under uncertain disturbance.



(a) Trajectories of the USV–UAV system in the horizontal plane



(b) Time responses of formation tracking errors

Figure 7 Comparison of the simulation results

5 Conclusions

This article investigates a distributed adaptive TFT regulation control scheme for USV– UAV systems subject to unknown external disturbances. The control framework is established by output redefinition-based dynamic transformation and a double-loop control structure. A distributed observer is then developed to estimate the global states of all leaders. Inspired by the MLP-based RBFNN, an adaptive TFT control strategy is designed within the output regulation framework. In particular, adaptive laws are introduced to enhance the robustness of the control scheme. The effectiveness of the proposed control scheme is confirmed by Lyapunov stability analyses and numerical simulations. Despite its advantages, the proposed strategy has certain limitations. Notably, the selection of parameters, such as observer gains and regulation matrices, still depends

on the dynamics of the leaders. Therefore, future research will consider the full nonlinear dynamics of USV–UAV systems under leader uncertainty or in leaderless configurations. Moreover, leveraging the spatial mobility advantages of UAVs remains a challenging yet promising direction for future exploration.

Funding Supported by the National Key Research and Development Program of China (2021YFC2803400).

Acknowledgement This work was supported by the National Key Laboratory of Autonomous Marine Vehicle Technology and the Yangtze Delta Region Advanced Research Institute of Harbin Engineering University. The authors would like to express their sincere gratitude to the Editor-in-Chief and anonymous reviewers whose constructive comments have helped us to significantly improve both the technical quality and presentation of this manuscript.

Competing interests The authors have no competing interests to declare that are relevant to the content of this article.

References

Barrera C, Padron I, Luis F, Llinas O (2021) Trends and challenges in unmanned surface vehicles (USV): From survey to shipping. TransNav: International Journal on Marine Navigation and Safety of Sea Transportation 15(1): 135-142. DOI: 10.12716/1001.15.01.13

Bi W, Zhang M, Chen H, Zhang A (2024) Cooperative task allocation method for air-sea heterogeneous unmanned system with an application to ocean environment information monitoring. Ocean Engineering 309: 118496. DOI: 10.1016/j.oceaneng.2024.118496

Bounemeur A, Chemachema M (2021) Adaptive fuzzy fault-tolerant control using Nussbaum-type function with state-dependent actuator failures. Neural Computing and Applications 33: 191-208. DOI: 10.1007/s00521-020-04977-6

Bounemeur A, Chemachema M (2025) Finite-time output-feedback fault tolerant adaptive fuzzy control framework for a class of MIMO saturated nonlinear systems. International Journal of Systems Science 56(4): 733-752. DOI: 10.1080/00207721.2024.2409853

Bounemeur A, Chemachema M, Essounbouli N (2018) Indirect adaptive fuzzy fault-tolerant tracking control for MIMO nonlinear systems with actuator and sensor failures. ISA Transactions 79: 45-61. DOI: 10.1016/j.isatra.2018.04.014

Bounemeur A, Chemachema M, Zahaf A, Bououden S (2019) Adaptive fuzzy fault-tolerant control using Nussbaum gain for a class of SISO nonlinear systems with unknown directions. Proceedings of the 4th International Conference on Electrical Engineering and Control Applications, ICEECA, Constantine, Algeria, 493-510e. DOI: 10.1007/978-981-15-6403-1_34

Chang HC, Hsu YL, Hung SS, Ou GR, Wu JR, Hsu C Autono (2021) Autonomous water quality monitoring and water surface cleaning for unmanned surface vehicle. Sensors 21(4): 1102. DOI: 10.3390/s21041102

Chen D, Liu X, Yu W (2020) Finite-time fuzzy adaptive consensus for heterogeneous nonlinear multi-agent systems. IEEE Transactions on Network Science and Engineering 7(4): 3057-3066. DOI: 10.1109/TNSE.2020.3013528

Dong X, Hu G (2017) Time-varying formation tracking for linear multiagent systems with multiple leaders. IEEE Transactions on Automatic Control 62(7): 3658-3664. DOI: 10.1109/TAC.2017.2673411

Du H, Wen G, Wu D, Cheng, Y, Lü J (2020) Distributed fixed-time consensus for nonlinear heterogeneous multi-agent systems. Automatica 113: 108797. DOI: 0.1016/j.automatica.2019.108797

Godsil C, Royle GF (2013) Algebraic graph theory (Vol. 207). Springer, New York, USA

Gonzalez-Garcia A, Miranda-Moya A, Castañeda H (2021) Robust visual tracking control based on adaptive sliding mode strategy: Quadrotor UAV-catamaran USV heterogeneous system. 2021 International Conference on Unmanned Aircraft Systems (ICUAS), Athens, Greece, 666-672. IEEE. DOI: 10.1109/ICUAS51884.2021.9476707

Hua Y, Dong X, Hu G, Li Q, Ren Z (2019) Distributed time-varying output formation tracking for heterogeneous linear multiagent systems with a nonautonomous leader of unknown input. IEEE Transactions on Automatic Control 64(10): 4292-4299. DOI: 10.1109/TAC.2019.2893978

Hua Y, Dong X, Li Q, Ren Z (2020) Distributed adaptive formation tracking for heterogeneous multiagent systems with multiple nonidentical leaders and without well-informed follower. International Journal of Robust and Nonlinear Control 30(6): 2131-2151. DOI: 10.1002/rnc.4891

Huang B, Peng H, Zhang C, Ahn CK (2024) Distributed optimal coordinated control for unmanned surface vehicles with interleaved periodic event-based mechanism. IEEE Transactions on Vehicular Technology 73(12): 18073-18086. DOI: 10.1109/TVT.2024.3432736

Jiang W, Liu K, Charalambous T (2022) Multi-agent consensus with heterogeneous time-varying input and communication delays in digraphs. Automatica 135: 109950. DOI: 10.1016/j.automatica.2021.109950

Johansen K, Dunne AF, Tu YH, Jones BH, McCabe MF (2022) Monitoring coastal water flow dynamics using sub-daily high-resolution SkySat satellite and UAV-based imagery. Water Research 219: 118531. DOI: 10.1016/j.watres.2022.118531

Kang CM, Yeh LC, Jie SYR, Pei TJ, Nugroho H (2020) Design of USV for search and rescue in shallow water. In: Chan, C.S., et al. Intelligent Robotics and Applications. ICIRA 2020. Lecture Notes in Computer Science 12595: 351-363. Springer, Cham. DOI: 10.1007/978-3-030-66645-3_30

Khalid A, Mushtaq Z, Arif S, Zeb K, Khan MA, Bakshi S (2023) Control schemes for quadrotor UAV: taxonomy and survey. ACM Computing Surveys 56(5): 1-32. DOI: 10.1145/3617652

Li J, Zhang G, Li B (2022a) Robust adaptive neural cooperative control for the USV–UAV based on the LVS-LVA guidance principle. Journal of Marine Science and Engineering 10(1): 51. DOI: 10.3390/jmse10010051

Li J, Zhang G, Shan Q, Zhang W (2022b) A novel cooperative design for USV–UAV systems: 3-D mapping guidance and adaptive fuzzy control. IEEE Transactions on Control of Network Systems 10(2): 564-574. DOI: 10.1109/TCNS.2022.3220705

Li J, Zhang G, Zhang W, Shan Q, Zhang W (2023a) Cooperative path following control of USV–UAVs considering low design complexity and command transmission requirements. IEEE Transactions on Intelligent Vehicles 9(1): 715-724. DOI: 10.1109/TIV.2023.3317336

Li J, Zhang G, Zhang X, Zhang W (2023b) Integrating dynamic event-triggered and sensor-tolerant control: Application to USV–

UAVs cooperative formation system for maritime parallel search. IEEE Transactions on Intelligent Transportation Systems 25(5): 3986-3998. DOI: 10.1109/TITS.2023.3326271

Li W, Ge Y, Ye G (2022c) UAV–USV cooperative tracking based on MPC. 2022 34th Chinese Control and Decision Conference (CCDC), Hefei, China, 4652-4657. IEEE. DOI: 10.1109/CCDC55256.2022.10034383

Liu F, Dong X, Yu J, Hua Y, Li Q, Ren Z (2022) Distributed Nash equilibrium seeking of N-coalition noncooperative games with application to UAV swarms. IEEE Transactions on Network Science and Engineering 9(4): 2392-2405. DOI: 10.1109/TNSE.2022.3163447

Liu H, Weng P, Tian X, Mai Q (2023) Distributed adaptive fixed-time formation control for UAV–USV heterogeneous multi-agent systems. Ocean Engineering 267: 113240. DOI: 10.1016/j.oceaneng.2022.113240

Lv Y, Li Z, Duan Z (2018) Distributed PI control for consensus of heterogeneous multiagent systems over directed graphs. IEEE Transactions on Systems, Man, and Cybernetics: Systems 50(4): 1602-1609. DOI: 10.1109/TSMC.2018.2792472

Ouyang Q, Wu Z, Cong Y, Wang Z (2023) Formation control of unmanned aerial vehicle swarms: A comprehensive review. Asian Journal of Control 25(1): 570-593. DOI: 10.1002/asjc.2806

Qin H, Chen X, Sun Y (2022) Adaptive state-constrained trajectory tracking control of unmanned surface vessel with actuator saturation based on RBFNN and tan-type barrier Lyapunov function. Ocean Engineering 253: 110966. DOI: 10.1016/j.oceaneng.2022.11096

Sendner FM (2022) An energy-autonomous UAV swarm concept to support sea-rescue and maritime patrol missions in the Mediterranean sea. Aircraft Engineering and Aerospace Technology 94(1): 112-123. DOI: 10.1108/AEAT-12-2020-0316

Shao G, Ma Y, Malekian R, Yan X, Li Z (2019) A novel cooperative platform design for coupled USV–UAV systems. IEEE Transactions on Industrial Informatics 15(9): 4913-4922. DOI: 10.1109/TII.2019. 2912024

Song Y, He L, Zhang D, Qian J, Fu J (2018) Neuroadaptive fault-tolerant control of quadrotor UAVs: A more affordable solution. IEEE transactions on neural networks and learning systems 30(7): 1975-1983. DOI: 10.1109/TNNLS.2018.2876130

Tian E, Li Y, Liao Y, Cao J (2024) UAV–USV docking control system based on motion compensation deck and attitude prediction. Ocean Engineering 307: 118223. DOI: 10.1016/j.oceaneng.2024.118223

Wang N, Ahn CK (2021) Coordinated trajectory-tracking control of a marine aerial-surface heterogeneous system. IEEE/ASME Transactions on Mechatronics 26(6): 3198-3210. DOI: 10.1109/TMECH.2021.3055450

Wu GX, Ding Y, Tahsin T, Atilla I (2023) Adaptive neural network and extended state observer-based non-singular terminal sliding modetracking control for an underactuated USV with unknown uncertainties. Applied Ocean Research 135: 103560. DOI: 10.1016/j.apor.2023.103560

Xu Y, Luo D, You Y, Duan H (2019) Distributed adaptive affine formation control for heterogeneous linear networked systems. IEEE Access 7: 23354-23364. DOI: 10.1109/ACCESS.2019.2898974

Yu Y, Guo J, Ahn C. K, Xiang Z (2022) Neural adaptive distributed formation control of nonlinear multi-UAVs with unmodeled dynamics. IEEE Transactions on Neural Networks and Learning Systems 34(11): 9555-9561. DOI: 10.1109/TNNLS.2022.3157079

Zain ZM, Watanabe K, Izumi K, Nagai I (2011) A nonholonomic control method for stabilizing an X4-AUV. Artificial Life and Robotics 16: 202-207. DOI: 10.1007/s10015-011-0918-8

Zhang F (2006) The Schur complement and its applications. Springer, New York, USA. https://doi.org/10.1007/b105056

Zhang H, Duan J, Wang Y, Gao Z (2019) Bipartite fixed-time output consensus of heterogeneous linear multiagent systems. IEEE Transactions on Cybernetics 51(2): 548-557. DOI: 10.1109/TCYB.2019.2936009